



The Orbital Histories of Magellanic Satellites Using *Gaia* DR2 Proper Motions

Ekta Patel^{1,2} , Nitya Kallivayalil³ , Nicolas Garavito-Camargo⁴ , Gurtina Besla⁴, Daniel R. Weisz¹ ,
Roeland P. van der Marel^{5,6} , Michael Boylan-Kolchin⁷ , Marcel S. Pawlowski⁸ , and Facundo A. Gómez^{9,10}

¹Department of Astronomy, University of California, Berkeley, 501 Campbell Hall, Berkeley, CA 94720, USA; ektapatel@berkeley.edu

²Miller Institute for Basic Research in Science, 468 Donner Lab, Berkeley, CA 94720, USA

³Department of Astronomy, University of Virginia, 530 McCormick Road, Charlottesville, VA 22904, USA

⁴Steward Observatory, University of Arizona, 933 North Cherry Avenue, Tucson, AZ 85721, USA

⁵Space Telescope Science Institute, 3700 San Martin Drive, Baltimore, MD 21218, USA

⁶Center for Astrophysical Sciences, Department of Physics & Astronomy, Johns Hopkins University, Baltimore, MD 21218, USA

⁷Department of Astronomy, The University of Texas at Austin, 2515 Speedway, Stop C1400, Austin, TX 78712-1205, USA

⁸Leibniz-Institut für Astrophysik Potsdam (AIP), An der Sternwarte 16, D-14482 Potsdam, Germany

⁹Instituto de Investigación Multidisciplinar en Ciencia y Tecnología, Universidad de La Serena, Raúl Bitrán 1305, La Serena, Chile

¹⁰Departamento de Astronomía, Universidad de La Serena, Av. Juan Cisternas 1200 Norte, La Serena, Chile

Received 2020 January 6; revised 2020 February 17; accepted 2020 February 27; published 2020 April 22

Abstract

With the release of *Gaia* DR2, it is now possible to measure the proper motions (PMs) of the lowest-mass, ultrafaint satellite galaxies in the Milky Way’s (MW) halo for the first time. Many of these faint satellites are posited to have been accreted as satellites of the Magellanic Clouds (MCs). Using their six-dimensional phase-space information, we calculate the orbital histories of 13 ultrafaint satellites and five classical dwarf spheroidal galaxies in a combined MW+LMC+SMC potential to determine which galaxies are dynamically associated with the MCs. These 18 galaxies are separated into four classes: (i) long-term Magellanic satellites that have been bound to the MCs for at least the last two consecutive orbits around the MCs (Carina 2, Carina 3, Horologium 1, Hydrus 1); (ii) Magellanic satellites that were recently captured by the MCs < 1 Gyr ago (Reticulum 2, Phoenix 2); (iii) MW satellites that have interacted with the MCs (Sculptor 1, Tucana 3, Segue 1); and (iv) MW satellites (Aquarius 2, Canes Venatici 2, Crater 2, Draco 1, Draco 2, Hydra 2, Carina, Fornax, Ursa Minor). Results are reported for a range of MW and LMC masses. Contrary to previous work, we find no dynamical association between Carina, Fornax, and the MCs. Finally, we determine that the addition of the SMC’s gravitational potential affects the longevity of satellites as members of the Magellanic system (long-term versus recently captured), but it does not change the total number of Magellanic satellites.

Unified Astronomy Thesaurus concepts: Local Group (929); Milky Way Galaxy (1054); Magellanic Clouds (990); Dwarf galaxies (416); Galaxy dynamics (591)

1. Introduction

In the hierarchical cold dark-matter paradigm, dark-matter halos of order $10^{11} M_{\odot}$ commonly contain tens of their own subhalos with sufficient gravitational potential to host luminous galaxies. The Large Magellanic Cloud (LMC) and M33 are the only two galaxies in the Local Group with halo masses in the $10^{11} M_{\odot}$ regime, and they also happen to be the most massive satellites of the MW and M31, respectively. As such, the LMC and M33 are expected to have entered the halos of the MW and M31 with a group of their own satellite galaxies (i.e., satellites of satellite galaxies; see D’Onghia & Lake 2008). Recent studies have quantified predictions for the populations of satellites expected around the LMC and M33, finding that each should host approximately 5–10 ultrafaint dwarf galaxies (UFDs) with $M_{*} \approx 10^2$ – $10^5 M_{\odot}$ (e.g., Sales et al. 2011, 2013; Dooley et al. 2017; Patel et al. 2018; Jahn et al. 2019) at minimum.

Nearly 30 new dwarf galaxies have recently been discovered in the vicinity of the Magellanic Clouds (MCs; Bechtol et al. 2015; Drlica-Wagner et al. 2015, 2016; Kim & Jerjen 2015; Kim et al. 2015; Koposov et al. 2015b; Laevens et al. 2015; Martin et al. 2015; Torrealba et al. 2016a, 2016b, 2018; Homma et al. 2018; Koposov et al. 2018). Furthermore, the timely second data release from the *Gaia* mission (*Gaia* Collaboration et al. 2018a) has enabled proper motion (PM) measurements for these ultrafaint satellites (Fritz et al. 2018;

Kallivayalil et al. 2018; Massari & Helmi 2018; Simon 2018; Pace & Li 2019), now making it possible to study their 3D kinematics and orbital histories in unprecedented detail. With this new data from *Gaia* DR2, several authors have aimed to identify the subset of known UFDs and classical dwarf spheroidal galaxies in the MW’s halo that were originally satellites of the MCs.

Kallivayalil et al. (2018) measured the PMs of 13 UFDs that also had radial velocity measurements using *Gaia* DR2. They compared the new 3D kinematics of UFDs to the tidal debris of a cosmological analog of the LMC to determine which UFDs have coincident kinematics with the LMC debris and found that four UFDs (Carina 2, Carina 3, Horologium 1, Hydrus 1) are likely members of the Magellanic system. For UFDs without measured radial velocities at that time, they used the simulation to predict the PMs and radial velocities of expected Magellanic debris, finding that a group of stars in Phoenix 2 have a PM in DR2 consistent with this prediction. Pardy et al. (2020) and Jahn et al. (2019) used the orbital poles of UFDs and classical satellites calculated with *Gaia* DR2 PMs to additionally conclude that Carina and Fornax are also potential Magellanic satellites.

Erkal & Belokurov (2019) used *Gaia* DR2 PMs for 25 UFD satellites and the classical dwarfs to integrate orbits backwards in time, or *rewind orbits*, in a combined MW+LMC potential. By calculating the orbital energy of these 25 galaxies relative to

the LMC 5 Gyr ago, they determined that six UFDs (Carina 2, Carina 3, Horologium 1, Hydrus 1, Reticulum 2, and Phoenix 2) are likely members of the Magellanic system. While these analyses have quantified the viability of satellites as members of the Magellanic system, none have accounted for the gravitational influence of the Small Magellanic Cloud (SMC), which is in a binary orbit with the LMC (Murai & Fujimoto 1980; Besla et al. 2012). In some studies (i.e., Kallivayalil et al. 2018; Jahn et al. 2019), the inclusion of the SMC is inhibited by the simulations in that finding a reasonable cosmological match to the MW+LMC+SMC system is rare (e.g., Boylan-Kolchin et al. 2011). In other cases (i.e., Erkal & Belokurov 2019), the SMC is omitted as a gravitational mass that exerts non-negligible forces on other galaxies, especially the UFDs. However, this dismisses the competing tidal effects between the interacting MCs, which, in addition to tides from the MW, can perturb the orbits of satellites in a nonnegligible way and potentially impact the total number of Magellanic satellites today.

Similarly, existing predictions for the total number of satellites hosted by the LMC and SMC today, in a Λ CDM paradigm, also omit the dynamical significance of the Clouds’ binary dynamics. Dooley et al. (2017) quantified the number of satellites expected around both the LMC and SMC under the assumption that each of the Clouds can be treated as an isolated halo. However, this assumption implies that the SMC continued to accrete substructures up until $z = 0$; whereas, if it were captured >5 Gyr ago by the LMC, its mass growth may have been truncated at the time of capture, and some of those SMC satellites might have been destroyed by the LMC. Thus, while the predictions in Dooley et al. (2017) are helpful benchmarks, they may overestimate the number and longevity of Magellanic satellites.

Jethwa et al. (2016) do consider the combined gravitational influence of the MW, LMC, and SMC to calculate the probabilities that the *Dark Energy Survey* UFDs belong to the LMC and SMC. This work came before PMs were available; yet, they conclude that seven UFDs have a high probability ($p > 0.7$) for being satellites of the LMC.

The goal of this work is to use *Gaia* DR2 PMs to calculate the orbital histories of all potentially associated Magellanic satellites, selected based on their membership to the MW’s Vast Polar Structure (Pawlowski et al. 2012), and thereby determine which satellites have a high probability of entering the MW’s halo as a group with the MCs. We further distinguish between the Magellanic satellites that have made only one passage around the LMC and those that evidence long-lived companionship. Our analysis explicitly includes the combined gravitational influence of the MW, LMC, and SMC for the first time. We also account for dynamical friction (DF) from both the MW and LMC, as well as the binary orbital history of the LMC–SMC and its subsequent effect on candidate Magellanic satellites.

This paper is organized as follows. Section 2 includes justification for our sample selection and the observational data adopted for these galaxies. Section 3 outlines the analytic orbital model and all model parameters for the MW, LMC, and SMC. It also discusses the orbits of the MCs. In Section 4, we analyze the orbital histories of all 18 candidate Magellanic satellites under the gravitational influence of the MW, MW+LMC, and MW+LMC+SMC. We also calculate the statistical significance of each candidate satellite’s orbital

histories accounting for the errors in PMs, line-of-sight velocities, and distances. Using these results, we define selection criteria to identify true Magellanic satellites. Section 5 includes a comparison to recent literature, a discussion on the mass of the MW and LMC, and how the inclusion of the SMC affects the results. Finally, in Section 5, we also demonstrate how smaller PM measurement uncertainties can affect a satellite’s membership to the Magellanic system. Section 6 provides a summary of our conclusions.

2. Data

Here, we briefly describe the selection of satellite galaxies included in our sample and the data used in this study.

2.1. Sample Selection

Since Lynden-Bell (1976), it has been suggested that several of the MW’s classical dwarf satellites reside in a spatially coherent plane. More recent work has extended this plane to include several stellar streams and globular clusters. This is now referred to as the MW’s “Vast Polar Structure” (VPOS; Pawlowski et al. 2012). Our goal is to identify the orbital histories of satellites that are dynamical companions to the LMC and SMC today. Since the VPOS is coincident with the orbital plane of the MCs, high-probability members of the VPOS comprise our initial sample of possible Magellanic satellites.

In Fritz et al. (2018),¹¹ the following UFDs were identified as having $\geq 50\%$ probability of being members of the VPOS: Crater 2, Carina 2, Carina 3, Hydrus 1, Horologium 1, Reticulum 2, Tucana 3, Segue 1, Aquarius 2, and Canes Venatici 2. We also use the same criteria to choose the subset of classical satellites that lie in the VPOS: Carina, Draco, Fornax, Sculptor, and Ursa Minor. Pawlowski & Kroupa (2019) independently analyzed the disk of classical satellites in light of *Gaia* DR2 PMs and found that Leo II is also consistent with the VPOS but has a high orbital pole uncertainty given its large distance, so we omit Leo II from our sample.

In Kallivayalil et al. (2018), it was found that Hydra 2, Draco 2, and Phoenix 2 may also be associated with the MCs. Thus, we additionally include these three UFDs in our sample. For Phoenix 2, Kallivayalil et al. (2018) were able to measure a PM, but there was no measured radial velocity at the time. There is now a radial velocity measurement (Fritz et al. 2019) as well as an independent PM measurement for Phoenix 2 (Pace & Li 2019), allowing for a full exploration of its orbital history (see also Erkal & Belokurov 2019).

The total sample of candidate Magellanic satellites analyzed in this work is therefore comprised of 13 UFD satellites ($M_* \approx 10^2\text{--}10^5 M_\odot$) and five classical dwarf spheroidal satellites ($M_* \approx 10^5\text{--}10^7 M_\odot$). Their properties are listed in Tables 1 and 5. In the sections that follow, we will discuss the methods used to measure PMs and our selection of PM measurements for satellites where multiple measurements have been published.

2.2. Proper Motions of the Candidate Magellanic Satellites

Several groups measured PMs for MW dwarf galaxies with *Gaia* DR2. Given the difficulty in identifying member stars for

¹¹ We selected all satellites that have $p(\text{inVPOS}) \geq 0.5$ in Table 4 of Fritz et al. (2018).

Table 1
Properties of the Candidate Magellanic Satellites

Name	$m - M$	R.A. (deg)	Decl. (deg)	V_{LOS} (km s ⁻¹)	μ_{α}^* (mas yr ⁻¹)	μ_{δ} (mas yr ⁻¹)	$C_{\mu_{\alpha}, \mu_{\delta}}$ (mas yr ⁻¹)	Notes
UFDs								
Aquarius 2	20.16 ± 0.07	338.5	-9.3	-71.1 ± 2.5	-0.252 ± 0.526	0.011 ± 0.448	0.131	DM: (12); PM: (2); RV: (12)
Canes Ventici 2	21.02 ± 0.06	194.3	34.3	-128.9 ± 1.2	-0.342 ± 0.232	-0.473 ± 0.169	-0.006	DM: (13); PM: (2); RV: (32)
Carina 2	17.79 ± 0.05	114.1	-58.0	477.2 ± 1.2	1.79 ± 0.06	0.01 ± 0.05	0.03	DM: (14); PM: (3); RV: (33)
Carina 3	17.22 ± 0.1	114.6	-57.9	284.6 ± 3.4	3.046 ± 0.119	1.565 ± 0.135	0.066	DM: (14); PM: (2); RV: (33)
Crater 2	20.25 ± 0.1	177.3	-18.4	87.5 ± 0.4	-0.184 ± 0.061	-0.106 ± 0.031	-0.041	DM: (15); PM: (2); RV: (34)
Draco 2	16.66 ± 0.04	238.2	64.6	-347.6 ± 1.8	1.242 ± 0.276	0.845 ± 0.285	-0.591	DM: (16); PM: (2); RV: (35)
Horologium 1	19.6 ± 0.2	43.9	-54.1	112.8 ± 2.6	0.891 ± 0.088	-0.55 ± 0.08	0.294	DM: (17,18); PM: (2); RV: (36)
Hydrus 1	17.2 ± 0.04	37.4	-79.3	80.4 ± 0.6	3.733 ± 0.038	-1.605 ± 0.036	0.264	DM: (20); PM: (2); RV: (20)
Hydra 2	20.89 ± 0.12	185.4	-32.0	303.1 ± 1.4	-0.416 ± 0.519	0.134 ± 0.422	-0.427	DM: (19); PM: (2); RV: (37)
Phoenix 2	19.6 ± 0.2	355	-54.4	-42 ± 6	0.49 ± 0.11	-1.03 ± 0.12	-0.48	DM: (21); PM: (4); RV: (11)
Reticulum 2	17.5 ± 0.1	53.9	-54.0	62.8 ± 0.5	2.33 ± 0.07	-1.33 ± 0.08	0.06	DM: (21); PM: (3); RV: (38)
Segue 1	16.8 ± 0.2	151.8	16.1	208.5 ± 0.9	-1.697 ± 0.195	-3.501 ± 0.175	-0.087	DM: (22); PM: (2); RV: (39)
Tucana 3	16.8 ± 0.1	359.1	-59.6	-102.3 ± 2	-0.025 ± 0.034	-1.661 ± 0.035	-0.401	DM: (21); PM: (2); RV: (40,41)
Classical dwarfs								
Carina 1	20.0 ± 0.08	100.4	-51.0	229.1 ± 0.1	0.495 ± 0.015	0.143 ± 0.014	-0.08	DM: (23,24); PM: (1); RV: (42)
Draco 1	19.49 ± 0.17	260.1	57.9	-291.0 ± 0.1	-0.019 ± 0.009	-0.145 ± 0.01	-0.08	DM: (25,26); PM: (1); RV: (43)
Fornax 1	20.72 ± 0.04	40.0	-34.4	55.3 ± 0.3	0.376 ± 0.003	-0.413 ± 0.003	-0.09	DM: (27); PM: (1); RV: (42,44)
Sculptor 1	19.64 ± 0.13	15.0	-33.7	111.4 ± 0.1	0.082 ± 0.005	-0.131 ± 0.004	0.23	DM: (28,29); PM: (1); RV: (42,44)
Ursa Minor 1	19.4 ± 0.11	227.3	67.2	-246.9 ± 0.1	-0.182 ± 0.01	0.074 ± 0.008	-0.34	DM: (30,31); PM: (1); RV: (45)
LMC	18.50 ± 0.1	78.76	-69.19	262.2 ± 3.4	-1.910 ± 0.020	0.229 ± 0.047	...	DM:(5); PM:(6); RV:(7)
SMC	18.99 ± 0.1	13.18	-72.83	145.6 ± 0.6	-0.83 ± 0.02	-1.21 ± 0.01	...	DM:(8); PM:(9); RV:(10)

Note. Column 1: distance modulus, Column 2 and 3: R.A. and decl., Column 4: line-of-sight velocity, Column 5 and 6: PMs in the R.A. and decl. directions (without the additional systematic error included), Column 7: the covariance between the two PM components, Column 8: original reference for each measurement. References: (1) Gaia Collaboration et al. (2018b), (2) Fritz et al. (2018), (3) Massari & Helmi (2018), (4) Pace & Li (2019), (5) Freedman et al. (2001), (6) Kallivayalil et al. (2013), (7) van der Marel et al. (2002), (8) Cioni et al. (2000), (9) Zivick et al. (2018), (10) Harris & Zaritsky (2006), (11) Fritz et al. (2019), (12) Torrealba et al. (2016b), (13) Greco et al. (2008), (14) Torrealba et al. (2018), (15) Joo et al. (2018), (16) Longeard et al. (2018), (17) Koposov et al. (2015a), (18) Bechtol et al. (2015), (19) Vivas et al. (2016), (20) Koposov et al. (2018), (21) Mutlu-Pakdil et al. (2018), (22) Belokurov et al. (2007), (23) Coppola et al. (2015), (24) Vivas & Mateo (2013), (25) Bonanos et al. (2004), (26) Kinemuchi et al. (2008), (27) Rizzi et al. (2007), (28) Martínez-Vázquez et al. (2016), (29) Pietrzyński et al. (2008); [30] Carrera et al. (2002), (31) Bellazzini et al. (2002), (32) Simon & Geha (2007), (33) Li et al. (2018a), (34) Caldwell et al. (2017), (35) Martin et al. (2016), (36) Koposov et al. (2015b), (37) Kirby et al. (2015), (38) Simon et al. (2015), (39) Simon et al. (2011), (40) Simon et al. (2017), (41) Li et al. (2018b), (42) Walker et al. (2009a), (43) Walker et al. (2015), (44) Battaglia et al. (2012), (45) Kirby et al. (2010).

these relatively sparse dwarf galaxy systems from the larger MW foreground, some works took the approach of cross-matching publicly available spectroscopic member catalogs with DR2 (Fritz et al. 2018; Simon 2018), while others added photometric members under the assumption that member stars move coherently, forming a clump in PM space, and utilizing the position in the color-magnitude diagram (Gaia Collaboration et al. 2018b; Kallivayalil et al. 2018; Massari & Helmi 2018; Pace & Li 2019).

We start with the values from Fritz et al. (2018), who presented PMs for all dwarf galaxies in the MW vicinity based on cross-matching confirmed spectroscopic member stars for these dwarfs with *Gaia* DR2. They also presented the covariances of their reported errors. For dwarfs where additional photometric members are identified, we use PMs and reported errors from the measurement using more member stars, as well as the corresponding covariances (specifically from Gaia Collaboration et al. 2018b; Massari & Helmi 2018; Pace & Li 2019). We add a systematic error floor of 0.035 mas to all reported errors as in Fritz et al. (2018). Table 1 lists the PMs, line-of-sight velocities, and distance moduli for all satellites in our sample, including references to the original measurements.

The LMC and SMC PMs and measurement errors are taken from Kallivayalil et al. (2013) and Zivick et al. (2018), respectively. The LMC measurement is based on multiple epochs of *Hubble Space Telescope* (*HST*) data for 22 fields across the galaxy, separated by a 3–7 yr baseline, and centered on an inertial reference frame made up of background quasars. The long time baselines with *HST* lead to random errors of only 1%–2% per field. The SMC measurement is based on 35 *HST* fields, also centered on background quasars, and spanning a 3 yr baseline, as well as an additional eight *Gaia* DR1 stars. The PM measurements of both galaxies are consistent with the *Gaia* DR2 measurements (Gaia Collaboration et al. 2018b).

Galactocentric quantities are calculated using the same Cartesian coordinate system (X, Y, Z) as in Kallivayalil et al. (2013). In this system, the origin is at the Galactic center, the X -axis points in the direction from the Sun to the Galactic center, the Y -axis points in the direction of the Sun’s Galactic rotation, and the Z -axis points toward the Galactic north pole. The position and velocity of the dwarfs in this frame can be derived from the observed sky positions, distances, line-of-sight velocities, and PMs. Errors in the Galactocentric quantities are calculated by doing 1000 Monte Carlo drawings over the

Table 2
Galactocentric Properties of Candidate Magellanic Satellites

	X (kpc)	Y (kpc)	Z (kpc)	V_x (km s ⁻¹)	V_y (km s ⁻¹)	V_z (km s ⁻¹)
Aqu2	28.71 ± 1.23	53.16 ± 1.77	-85.98 ± 2.87	91.31 ± 239.21	250.76 ± 212.3	130.49 ± 166.0
CanVen2	-16.37 ± 0.22	18.58 ± 0.51	158.67 ± 4.32	-0.66 ± 162.9	-203.05 ± 150.42	-70.09 ± 16.93
Car2	-8.3 ± 0.0	-34.54 ± 0.8	-10.65 ± 0.25	134.12 ± 11.0	-287.58 ± 4.14	134.95 ± 13.02
Car3	-8.29 ± 0.0	-26.6 ± 1.24	-8.06 ± 0.37	-10.7 ± 18.9	-151.85 ± 8.41	356.05 ± 25.9
Cra2	10.3 ± 0.88	-81.23 ± 3.86	75.13 ± 3.57	-34.4 ± 35.2	115.88 ± 21.41	2.83 ± 19.96
Dra2	-10.57 ± 0.04	15.58 ± 0.28	14.61 ± 0.26	22.54 ± 22.16	100.31 ± 22.35	-341.04 ± 25.48
Hor1	-7.16 ± 0.1	-48.01 ± 4.36	-67.91 ± 6.16	-20.24 ± 30.24	-150.18 ± 45.34	152.34 ± 32.09
Hyl1	1.87 ± 0.19	-19.59 ± 0.36	-16.48 ± 0.3	-144.15 ± 6.58	-178.7 ± 8.73	288.26 ± 8.57
Hya2	47.82 ± 3.06	-117.14 ± 6.39	76.34 ± 4.17	-165.16 ± 302.26	-92.01 ± 257.22	208.27 ± 275.52
Phx2	25.47 ± 3.14	-24.81 ± 2.31	-71.85 ± 6.69	-67.68 ± 48.82	-165.47 ± 54.59	162.72 ± 31.4
Ret2	-9.63 ± 0.06	-20.38 ± 0.96	-24.14 ± 1.14	19.92 ± 12.38	-96.74 ± 17.42	218.24 ± 14.63
Seg1	-19.38 ± 0.98	-9.47 ± 0.84	17.67 ± 1.57	-98.19 ± 18.34	-205.06 ± 38.14	-35.49 ± 22.9
Tuc3	0.79 ± 0.41	-8.95 ± 0.4	-19.03 ± 0.85	23.48 ± 5.94	146.27 ± 8.05	185.68 ± 5.69
Car1	-24.72 ± 0.6	-94.62 ± 3.48	-39.26 ± 1.44	-36.84 ± 18.42	-50.55 ± 8.51	149.23 ± 20.28
Dra1	-4.15 ± 0.32	64.88 ± 5.0	45.01 ± 3.47	54.29 ± 13.85	4.15 ± 8.25	-151.78 ± 11.73
Fnx1	-39.58 ± 0.57	-48.15 ± 0.87	-126.93 ± 2.3	38.14 ± 22.76	-107.56 ± 21.25	76.0 ± 9.72
Scu1	-5.22 ± 0.19	-9.59 ± 0.6	-84.12 ± 5.26	16.93 ± 12.7	175.89 ± 16.04	-96.14 ± 1.87
UMin1	-22.16 ± 0.71	52.0 ± 2.68	53.46 ± 2.75	-4.26 ± 10.75	46.77 ± 10.69	-148.2 ± 10.61
LMC	-1.06 ± 0.33	-41.05 ± 1.89	-27.83 ± 1.28	-57.60 ± 7.99	-225.96 ± 12.60	221.16 ± 16.68
SMC	15.05 ± 1.07	-38.10 ± 1.75	-44.18 ± 2.03	17.66 ± 3.84	-178.60 ± 15.89	174.36 ± 12.47

Note. All quantities are calculated directly from the values compiled in Table 1. Solar reflex motion is taken from McMillan (2011) where $V_{c,peak}$ (8.29 kpc) \approx 239 km s⁻¹. We adopt the solar peculiar velocity from Schönrich et al. (2010) who find $(U, V, W)_\odot = (11.1^{+0.69}_{-0.75}, 12.24^{+0.47}_{-0.47}, 7.25^{+0.37}_{-0.36})$ km s⁻¹. Note the standard errors on each component represent the standard deviation from one iteration of the Monte Carlo scheme (i.e., 1000 random samples). The horizontal line indicates the division between ultrafaint galaxies and the classical satellite galaxies. Galaxies will appear in this order in tables moving forward.

errors in the measured PMs (including reported covariances), radial velocities, and distance moduli. The Local Standard of Rest velocity at the solar circle from McMillan (2011) and solar peculiar velocity from Schönrich et al. (2010) are used in the transformation from sky coordinates to Galactocentric coordinates (see caption for Table 2).

Table 2 provides the Cartesian Galactocentric quantities for each satellite galaxy in our sample. The errors on each position and velocity component represent the standard deviation on that quantity derived from 1000 Monte Carlo samples.

3. Analytic Orbital Models

In this section, we briefly describe the method used to calculate orbital histories for all satellites in our sample using the Galactocentric positions and velocities provided in Table 2 as initial conditions. This method follows the general strategies outlined in Kallivayalil et al. (2013), Gómez et al. (2015), and further modified in Patel et al. (2017, hereafter P17).

3.1. Galaxy Potentials

To numerically integrate orbits backwards in time, the gravitational potentials of the MW, LMC, SMC, and all satellites are modeled as extended mass distributions. The following subsections outline the specific parameters of each galactic potential.

3.1.1. Milky Way Potential

Two MW dark matter halo potentials are considered throughout this analysis to account for both a light and heavy MW scenario, identical to the MW models in P17. The light

MW mass model will be referred to as MW1 and has a virial mass¹² of $10^{12} M_\odot$ and virial radius of 261 kpc. The heavy MW mass potential, MW2, has a virial mass of $1.5 \times 10^{12} M_\odot$ and virial radius of 299 kpc.

Each MW potential is a composite of an Navarro–Frenk–White (NFW) halo (Navarro et al. 1996), a Miyamoto–Nagai disk (Miyamoto & Nagai 1975), and a Hernquist bulge (Hernquist 1990). The NFW dark matter halo is adiabatically contracted owing to the presence of the disk using the CONTRA code (Gnedin et al. 2004). The density profile of the MW’s halo is truncated at the virial radius of each model. Beyond the virial radius, the potential of the MW is treated as a point mass as in P17.

The MW’s disk mass in each model was chosen to provide the best match to the observed rotation curve from McMillan (2011), such that the peak velocity reaches $V_c \approx 239$ km s⁻¹ at the solar radius. Figure 1 in P17 illustrates the rotation curves of our adopted MW models. All MW halo, disk, and bulge parameters for each model are listed in Table 3.

3.1.2. LMC and SMC Potentials

The LMC potential is modeled using two components, namely a Hernquist halo and a Miyamoto–Nagai disk. We consider three total masses for the LMC at infall: 0.8, 1.8, $2.5 \times 10^{11} M_\odot$, which will be referred to as LMC1, LMC2, and LMC3, respectively. The mass of the LMC’s disk is held fixed at its present day stellar mass $M_d = 3 \times 10^9 M_\odot$ (van der Marel et al. 2002) for all three models, and the

¹² We adopt the Bryan & Norman (1998) definition of virial mass using $\Omega_m = 0.27$, $h = 0.7$, and $\Delta_{vir} = 359$.

Table 3
Parameters for Each MW Mass Model

	MW1	MW2
$M_{\text{vir}} (10^{10} M_{\odot})$	100	150
$R_{\text{vir}} (\text{kpc})$	261	299
c_{vir}	9.86	9.56
$M_{\text{d}} (10^{10} M_{\odot})$	6.5	5.5
$R_{\text{d}} (\text{kpc})$	3.5	3.5
$z_{\text{d}} (\text{kpc})$	0.53	0.53
$M_{\text{b}} (10^{10} M_{\odot})$	1	1
$R_{\text{b}} (\text{kpc})$	0.7	0.7

Note. These are identical to the MW models in P17. From top to bottom the rows list: (1) virial mass following the Bryan & Norman (1998) definition, (2) virial radius calculated with Equation A1 from van der Marel et al. (2012b), (3) virial concentration, (4) stellar disk mass, (5) stellar disk radial scale length, (6) stellar disk scale height, (7) bulge mass, and (8) bulge scale length.

Table 4
Parameters for the LMC and SMC Mass Models

	LMC 1	LMC2 ^a	LMC3	SMC1	SMC2
$M_{\text{H}} (10^{10} M_{\odot})$	8	18	25	0.5	3
$R_{\text{vir}} (\text{kpc})$	113	148	165	45	81
$r_{\text{H}} (\text{kpc})$	12.5	23.1	28.8	2.5	8.6
$M_{\text{d}} (10^9 M_{\odot})$	3	3	3
$R_{\text{d}} (\text{kpc})$	1.7	1.7	1.7
$z_{\text{d}} (\text{kpc})$	0.27	0.27	0.27

Notes. The LMC is a two-component disk+halo potential and the SMC is only modeled as a Hernquist sphere. From top to bottom, the rows list: (1) Hernquist halo mass, (2) virial radius, (3) Hernquist scale radius, (4) stellar disk mass, (5) stellar disk radial scale length, and (6) stellar disk scale height.

^a Indicates the fiducial LMC model.

Hernquist halo scale radius is varied to match the rotation velocity of $V_c \approx 92 \text{ km s}^{-1}$ at 8.7 kpc (van der Marel & Kallivayalil 2014). All LMC model parameters are listed in Table 4.

As in Garavito-Camargo et al. (2019), the majority of this work will focus on the intermediate mass LMC2, our fiducial LMC model. This mass is consistent with recent models of the Magellanic system and with the halo mass estimates from abundance matching (Besla et al. 2012, 2013, 2016). However, we will discuss the effects of a lower (LMC1) and higher (LMC3) LMC mass model throughout this analysis.

The SMC is modeled as a Hernquist halo since its baryonic content is much less massive than the LMC's, owing to repeated encounters with the LMC (Besla et al. 2012). Such encounters also imply the halo of the SMC is truncated today. The Hernquist halo scale radius (r_{H}) is determined by matching the mass profile to the dynamical mass within 3 kpc of the center of the SMC, $M(3 \text{ kpc}) \approx 2 \times 10^9 M_{\odot}$ (Harris & Zaritsky 2006). Di Teodoro et al. (2019) find that a dynamical mass within 4 kpc of $M(4 \text{ kpc}) \approx 1\text{--}1.5 \times 10^9 M_{\odot}$, is required to reproduce the SMC's rotation curve. Our models are therefore representative of the SMC's current properties. We consider two different SMC models with halo masses of $5 \times 10^9 M_{\odot}$ (SMC1) and $3 \times 10^{10} M_{\odot}$ (SMC2), respectively. For such halo masses, the SMC's baryon fraction is 5% (excluding the gas content of the

Table 5
Absolute Magnitude, Size, and Velocity Dispersion of Candidate Magellanic Satellites

	M_V	$R_{1/2}$ (pc)	σ (km s^{-1})	References ^a
Aqu2	-4.36 ± 0.14	160 ± 26	$5.4^{+3.4}_{-0.9}$	(12), (12), (12)
CanVen2	-5.17 ± 0.32	71 ± 11	4.6 ± 1.0	(46), (46), (32)
Car2	-4.50 ± 0.10	92 ± 8	$3.4^{+1.2}_{-0.8}$	(14), (14), (33)
Car3	-2.4 ± 0.20	30 ± 8	$5.6^{+4.3}_{-2.1}$	(14), (14), (33)
Cra2	-8.20 ± 0.10	1066 ± 86	2.7 ± 0.3	(47), (47), (34)
Dra2	$-0.80^{+0.40}_{-1.00}$	19^{+4}_{-3}	< 5.9	(16), (16), (16)
Hor1	-3.76 ± 0.56	40^{+1}_{-9}	$4.9^{+2.8}_{-0.9}$	(46), (46), (36)
Hyl1	-4.71 ± 0.08	53 ± 4	$2.7^{+0.5}_{-0.4}$	(20), (20), (20)
Hya2	-4.86 ± 0.37	67 ± 13	< 3.6	(46), (46), (37)
Phx2	-2.70 ± 0.40	37 ± 8	...	(21), (21), ...
Ret2	-3.88 ± 0.38	51 ± 3	3.3 ± 0.7	(46), (46), (38)
Seg1	-1.30 ± 0.73	24 ± 4	$3.7^{+1.4}_{-1.1}$	(46), (46), (39)
Tuc3	-1.49 ± 0.20	37 ± 9	< 1.2	(21), (21), (40)
Car1	-9.45 ± 0.05	349 ± 4	6.6 ± 1.2	(46), (46), (48)
Dra1	-8.88 ± 0.05	219 ± 2	9.1 ± 1.2	(46), (46), (42)
Fnx1	-13.34 ± 0.14	787 ± 9	11.7 ± 0.9	(46), (49), (42)
Scu1	-10.82 ± 0.14	308 ± 1	9.2 ± 1.1	(46), (46), (42)
UMin1	-9.03 ± 0.05	383 ± 2	9.5 ± 1.2	(46), (46), (50)

Note.

^a Reference numbers correspond to the reference list provided at the end of Table 1. Additional references include: (46) Muñoz et al. (2018), (47) Torrealba et al. (2016a), (48) Walker et al. (2008), (49) Battaglia et al. (2006), (50) Walker et al. (2009b).

Magellanic Stream; Besla 2015). The model parameters for the SMC potentials are listed in Table 4.

3.1.3. Classical Satellites

All classical satellites considered in this work have stellar masses in the range $M_* = 10^5\text{--}10^7 M_{\odot}$. As such, the dark matter halos of all classical satellites fainter than the MCs are modeled as Plummer spheres (Plummer 1911) with a total halo mass of $10^{10} M_{\odot}$ (see Bullock & Boylan-Kolchin 2017). The Plummer scale radius for each classical satellite is determined by computing the radius at which the halo mass enclosed within the Plummer profile matches the dynamical mass inferred at the half-light radius. The half-light radii and stellar velocity dispersions used to compute dynamical masses, which are derived from the Walker et al. (2009b) dynamical mass estimator, are compiled in Table 5. The resulting Plummer scale radii (r_p) for the classical satellites are as follows: Carina (4.0 kpc), Draco (2.1 kpc), Fornax (4.4 kpc), Sculptor (2.7 kpc), and Ursa Minor (3.9 kpc).

3.1.4. Ultrafaint Satellites

UFDs, as their name suggests, are much fainter and have significantly lower stellar masses than the classical dwarfs ($M_* = 10^2\text{--}10^5$ versus $M_* = 10^5\text{--}10^7$). UFDs are also significantly smaller in size with half-light radii typically $\lesssim 200$ pc and stellar velocity dispersions $\lesssim 5 \text{ km s}^{-1}$. Table 5 lists the absolute magnitudes, half-light radii, and stellar velocity dispersions for UFD galaxies in our sample.

Given their low stellar masses, UFDs are also modeled as Plummer spheres but with a total halo mass of $10^9 M_{\odot}$.

(Jeon et al. 2017). Applying the Walker et al. (2009b) mass estimator to the measured velocity dispersion and half-light radii of Aqu2, Ret2, and Hor1, and searching for the radius at which the mass enclosed within a Plummer profile is equivalent to the dynamical mass yields scale radii of 1.2, 0.8, and 0.6 kpc for these satellites, respectively. Thus, all UFDs are assigned the same Plummer scale radius of 1 kpc for simplicity since velocity dispersion values are unavailable or uncertain for some UFDs in our sample (see Table 5). Since Crater 2 (Cra2) is a known outlier on the size–luminosity relation with a size similar to Fornax and the SMC but a luminosity that is consistent with the UFD satellites (Torrealba et al. 2016a, see Table 5), we adopt a more appropriate Plummer scale radius of 9 kpc for Cra2.

3.2. DF and Numerical Integration Scheme

3.2.1. Acceleration from the MW

We present orbital solutions for each candidate Magellanic satellite galaxy in three different scenarios. First, we calculate the orbit of each satellite in the presence of the MW only. Then we consider the combined MW and LMC potential. Finally, we add the SMC and calculate orbits in the full MW+LMC+SMC potential. The progression of adding one galactic potential at a time allows us to disentangle the influence of each additional massive body. In every scenario, each galaxy experiences the gravitational influence of every other galaxy (up to $N_{\text{gal}} = 4$). Though its gravitational potential is static, the MW’s center of mass is not held fixed and, therefore, moves in response to the LMC’s close passage as in Gómez et al. (2015) and P17.

Satellites passing through the halo of the MW experience DF as approximated by the Chandrasekhar formula (Chandrasekhar 1943):

$$\mathbf{F}_{\text{df}} = -\frac{4\pi G^2 M_{\text{sat}}^2 \ln\Lambda \rho(r)}{v^2} \left[\text{erf}(X) - \frac{2X}{\sqrt{\pi}} \exp(-X^2) \right] \frac{\mathbf{v}}{v}. \quad (1)$$

Here, $\rho(r)$ is the density of the MW’s adiabatically contracted dark matter halo at a distance r from the Galactic center. $X = v/\sqrt{2\sigma}$ where σ is the one-dimensional galaxy velocity dispersion for an NFW halo derived in Zentner & Bullock (2003). DF also depends on the total mass of the satellite M_{sat} as well as its total velocity v . The Coulomb logarithm ($\ln\Lambda$) is calibrated with respect to each class of satellite (i.e., massive satellites like the LMC, classical satellites including the SMC, and UFDs). For all MW–LMC acceleration calculations, we adopt the Coulomb parameterization in van der Marel et al. (2012a):

$$\ln\Lambda = \max[L, \ln(r/Ca_s)^\alpha], \quad (2)$$

where $L = 0$, $C = 1.22$, $\alpha = 1.0$. These values are constants that parameterize the best-fitting match for the orbit of a 1:10 host-satellite mass ratio from N -body simulations. a_s is the scale radius of the satellite, which is the Hernquist scale length (r_{H}) or Plummer scale length (r_{p}) depending on the satellite’s potential.

We adopt the Coulomb logarithm from Hashimoto et al. (2003) for the DF approximation used for the SMC, the classical satellites, and the UFDs as they move through the

MW’s halo:

$$\ln\Lambda = \frac{r}{1.4 a_s}, \quad (3)$$

where a_s is once again the satellite scale radius and r is the distance of the satellite from the MW’s Galactic Center. The total acceleration felt by all satellites owing to the MW only is then:

$$\ddot{\mathbf{r}}_{\text{sat,MW}} = \frac{d\Phi_{\text{bulge,MW}}}{dr} + \frac{d\Phi_{\text{disk,MW}}}{dr} + \frac{d\Phi_{\text{halo,MW}}}{dr} + \frac{\mathbf{F}_{\text{df}}}{M_{\text{sat}}} \quad (4)$$

and the total acceleration felt by the MW as a result of each satellite is:

$$\ddot{\mathbf{r}}_{\text{MW}} = \frac{d\Phi_{\text{sat}}}{dr}. \quad (5)$$

Note that in the case of the LMC, the MW will experience two acceleration forces since the LMC is modeled as a disk plus halo potential (i.e., $\Phi_{\text{LMC}} = \Phi_{\text{disk}} + \Phi_{\text{halo}}$).

3.2.2. Acceleration from the LMC

Since the LMC is 8–25 times more massive than the classical satellites and 80–250 times more massive than the UFDs in our models, it too will exert a drag force that slows the orbital motion of satellites that pass through regions where the LMC’s halo DM density is in excess of the ambient MW halo. As we calculate orbits backwards in time, DF translates to an acceleration force. This is accounted for using the same DF approximation adopted in Bekki & Chiba (2005) and Besla et al. (2007) to account for the effect of the SMC passing through the LMC’s halo.

$$\mathbf{F}_{\text{df,LMC}} = 0.428 \ln\Lambda \frac{GM_{\text{sat}}^2}{r^2}. \quad (6)$$

Here, r is now the distance between the satellite and the center of the LMC and $\ln\Lambda = 0.3$ (instead of $\ln\Lambda = 0.2$ as in Besla et al. 2007). This value for $\ln\Lambda$ was chosen by finding the best analytic match to the LMC–SMC orbit from N -body simulations, prior to accretion by the MW (Besla et al. 2010, 2012). Between SMC1 and SMC2, we find that SMC1 provides the better fit to this simulated orbit and will use it as the fiducial SMC model throughout this analysis.

The DF approximation given in Equation (6) is applied to all candidate Magellanic satellites in addition to the SMC when they fall within the region of the LMC’s halo where its density dominates over the MW’s. This radius is determined by finding the distance at which the density profile of the MW (as described in Section 3.1.1) is equivalent to the LMC’s density profile (as described in Section 3.1.2). In doing so, we find two distances at which these quantities are equivalent, denoted as the *inner* and *outer* radius. These radii act as pseudotruncation radii; thus, DF owing to the LMC is only active when candidate Magellanic satellites or the SMC pass within the *outer* radius (r_{outer}) as listed in Table 6. The total acceleration felt by all satellites due to the LMC is summarized as

$$\ddot{\mathbf{r}}_{\text{sat,LMC}} = \frac{d\Phi_{\text{disk,LMC}}}{dr} + \frac{d\Phi_{\text{halo,LMC}}}{dr} + \frac{\mathbf{F}_{\text{df,LMC}}}{M_{\text{sat}}}. \quad (7)$$

Table 6
Radius Where the Density of the MW and the LMC Are Equal Today

MW1	r_{inner} (kpc)	r_{outer} (kpc)
LMC1	15.7	41.9
LMC2 ^a	16.9	60.8
LMC3	17.3	74.2
MW2	r_{inner} (kpc)	r_{outer} (kpc)
LMC1	16.3	46.1
LMC2 ^a	17.6	68.2
LMC3	18.0	84.2

Notes. DF due to galaxies passing through the LMC’s halo is implemented when satellites pass within r_{outer} .

^a Indicates the fiducial LMC model.

The LMC in turn experiences the acceleration of each satellite as in Equation (5) (replacing the MW subscript with the LMC). We have also checked whether any DF forces should be included for the UFD satellites as they pass through the halo of the SMC using the same prescription as in Equation (3), however, our tests showed that this effect is negligible so we have omitted it from our model.

3.3. Orbits of the Magellanic Clouds

As in P17, the symplectic leapfrog integration method from Springel et al. (2001) is used to numerically integrate the equations of motions backwards in time. Orbits are only calculated for the last 6 Gyr as the mass evolution of the MW and mass loss due to tides are not included in our framework. Furthermore, the Appendix of P17 showed that a 6 Gyr integration period provides a good match to corresponding orbits of satellite galaxies from a cosmological simulation, but that at earlier times, cosmological orbits begin to deviate from the analytic results. Second, Santistevan et al. (2020) found that MW-mass galaxies have acquired about 80% of their mass by 6 Gyr ago, so integrating further than this would require a more complex orbital model that handles the mass evolution of the MW. Finally, integrating for a shorter orbital period would not be ideal as it often takes $\sim 5\text{--}7$ Gyr for satellites to complete multiple orbits around the MW (and the MCs).

Orbits resulting from the positions and velocities in Table 2 will be referred to as *direct orbits*, i.e., the orbits calculated from the Galactocentric quantities derived directly from the transformation of average proper motion, line-of-sight velocity, and distance modulus to Cartesian coordinates centered on the MW as described in Section 2. These orbits do not represent the measurement errors on the observational quantities.

Figure 1 shows the orbit of the LMC relative to the MW for all three LMC models in both MW mass potentials. In MW1, all LMC mass models are on a first infall, long-period orbit with a recent pericenter occurring ~ 50 Myr ago. In the more massive MW2 potential, all LMC models complete two pericentric passages. The first occurred at ~ 4 Gyr ago at a distance of 100–150 kpc and the second occurred at ~ 50 Myr ago at approximately 50 kpc.

Figure 1 also shows the orbit of SMC1 (dashed lines) relative to the LMC in all three LMC models. The left panel shows orbits in the MW1 potential and the right panel shows the same orbits calculated in the MW2 potential. For both MW masses, the time and distance at the most recent LMC–SMC

pericentric passage are consistent with results from Zivick et al. (2018), who find an impact parameter of 7.5 ± 2.5 kpc at 147 ± 33 Myr ago.

The SMC completes multiple pericentric passages about the LMC for MW1, whereas the binary LMC–SMC orbit is disrupted at times earlier than 3 Gyr ago for MW2 (see also Bekki & Chiba 2005; Kallivayalil et al. 2013; Zivick et al. 2018). Kallivayalil et al. (2013) found that the latter solution is quite implausible and that an MW mass of $\lesssim 1.5 \times 10^{12} M_{\odot}$ is preferred to form a long-lived LMC–SMC binary. Given the extensive work that has been carried out on the orbit of the LMC–SMC system, we count the SMC as a satellite of the LMC moving forward.

4. Analysis of Orbital Histories

In this section, we present the direct orbital histories for all candidate Magellanic satellites. In Section 4.3, we present the statistical significance of these orbital solutions by calculating 1000 orbital histories for each candidate satellite using the fiducial LMC model and both MW masses. This analysis samples the 1σ error space of the PMs, line-of-sight velocities, and distance moduli. Finally, in Section 4.4 we identify which candidate Magellanic satellites exhibit orbital histories that confirm they are dynamically associated members of the Magellanic system accounting for both the latest PM measurements and the acceleration of the SMC for the first time.

4.1. Orbits of the Classical Satellites

Figure 2 shows direct orbits for the classical satellite galaxies in our sample. Note that all distances are shown relative to the Galactic Center. All blue lines correspond to MW1, while all orange lines correspond to MW2. This color scheme will remain fixed in all subsequent figures of orbital histories. The fiducial LMC mass model (LMC2) is adopted in all cases. We discuss how orbits evolve when the mass of the LMC is lower (LMC1) and higher (LMC3) in Section 4.4. Each satellite’s orbital history is calculated in three potentials: the MW only (dashed lines), the MW+LMC (solid lines), and the MW+LMC+SMC (dotted lines).

Since all of the classical dwarf spheroidal galaxies have PM measurements predating *Gaia* DR2, the left column of Figure 2 shows the direct orbits using the most recent pre-*Gaia* DR2 PM for each classical dwarf galaxy. These come from Sohn et al. (2017) for Draco and Sculptor, Piatek et al. (2005) for Ursa Minor, Piatek et al. (2003) for Carina, and Piatek et al. (2007) for Fornax, as denoted in the top right of each panel. The right column shows the direct orbits using the *Gaia* DR2 PMs from Gaia Collaboration et al. (2018b).

In the cases of Carina, Fornax, and Ursa Minor, the *Gaia* DR2 and preexisting PMs are consistent with each other at the 2σ level of the old measurement, although the latter have large error bars ($100\text{--}200 \mu\text{as yr}^{-1}$). The *Gaia* DR2 PMs for these galaxies reach much higher precision ($3\text{--}15 \mu\text{as yr}^{-1}$). Draco and Sculptor’s previous PM measurements were made using *HST* and a baseline of nearly 10 yr (Sohn et al. 2017); thus, the most recent PM measurements reach similar precision ($5\text{--}20 \mu\text{as yr}^{-1}$).

Overall, Figure 2 shows that all of the classical satellites are noticeably impacted by the gravitational influence of the LMC (dashed versus solid lines). This effect manifests in different ways for each individual classical satellite such that the

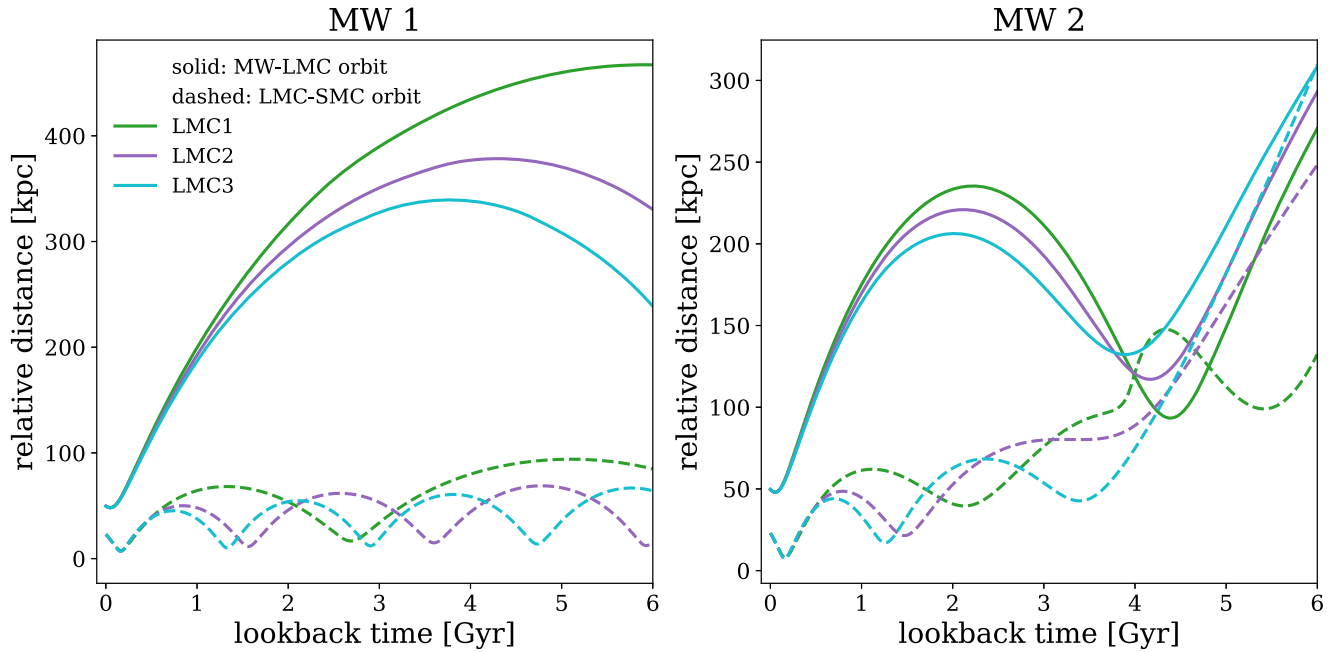


Figure 1. Direct orbits for the LMC (solid lines) relative to the MW and the SMC relative to the LMC (dashed lines). The left panel shows all orbits calculated for the low-mass MW1 model, while the right panel illustrates orbits in the high-mass MW2 model. All orbits are calculated in the combined MW+LMC+SMC potential. In MW1, the LMC is on a wide period orbit and only completes one pericentric passage in the last 6 Gyr regardless of LMC mass. The SMC makes multiple passes around the LMC in MW1. In MW2, the LMC completes two pericentric passages in the last 6 Gyr. The binary orbit of the LMC–SMC is disrupted at times greater than 3 Gyr ago in a high-mass MW model, shortly after the system makes a close encounter with the MW.

inclusion of the LMC can change the length of the orbital period, increase or decrease the distance at pericenter (apocenter), as well as alter the timing of pericenter (apocenter). However, the addition of the SMC (dotted lines) has little effect on the orbital properties of the classical satellites. This is not surprising since the adopted mass of the SMC is only 50% of the mass used for the classical satellite galaxies.

Figure 2 shows that Carina’s orbit is similar for the MW +LMC+SMC potential using both PMs. Adopting the *Gaia* DR2 PM leads to an orbital period that is larger by a factor of ~ 1.3 . Draco’s direct orbits are also consistent between the previous and *Gaia* DR2 PMs. The orbits have similar periods, and the most notable difference is a decrease in the distances achieved at apocenter by ~ 25 kpc using the *Gaia* DR2 PMs. There is little to no difference between the orbits calculated with previous and *Gaia* DR2 PMs for Ursa Minor and Sculptor.

Fornax shows the most significant differences between the previously measured and *Gaia* DR2 PMs. In the MW+LMC+SMC potential, Fornax’s *Gaia* DR2 orbit indicates that it has completed nearly two orbital passages in the last 6 Gyr with the most recent passage around the MW occurring at ~ 1.5 Gyr ago at a distance of 90–120 kpc, which is much closer than the orbit calculated using the Piatek et al. (2007) PMs. Carina and Fornax have recently been posited as satellites of the MCs (Jahn et al. 2019; Pardy et al. 2020). In Sections 4.3 and 4.4, we will explore the statistical likelihood of this based on their orbital histories relative to the LMC.

4.2. Orbits of the Ultrafaint Satellites

Figure 3 shows the direct orbits as a function of lookback time for all 13 UFD satellites in our sample. All colors and line styles represent the same model parameters as in Figure 2.

For every satellite with the exception of Seg1, there are noticeable differences in the resulting orbital histories when satellites experience only the MW’s gravity (dashed lines) versus the combined MW+LMC potential (solid lines). These differences manifest as changes in the orbital period, distance at pericenter and apocenter, as well as the timing of these critical orbital parameters. The inclusion of the LMC does not affect each satellite’s orbit in the same way. For example, including the influence of the LMC decreases the orbital period of Car2 by ~ 1 Gyr (for MW2) and increases the orbital period of Dra2 (for MW1 and MW2) by ~ 0.3 Gyr.

For Cra2, the impact of the LMC is different, such that it decreases the distance achieved at pericenter from ~ 30 kpc to ~ 10 kpc, making it well-aligned with previous conclusions that Cra2 may have suffered from extreme tidal stripping (Torrealba et al. 2016a; Fattahi et al. 2018; Sanders et al. 2018; Erkal & Belokurov 2019; Fu et al. 2019). Hyi1, Car3, Car2, Phx2, and Hor1 also exhibit noticeable perturbations when the LMC potential is included. These satellites have all previously been claimed to be Magellanic satellites by other authors (Kallivayalil et al. 2018; Erkal & Belokurov 2019; Jahn et al. 2019, see Section 5.1).

When the SMC’s potential is additionally included (dotted lines), the orbits of the satellites are further perturbed (see Jethwa et al. 2016). This is particularly interesting in the case of Ret2 where the orbital solution in the combined MW+LMC+SMC for the low-mass MW (MW1) shows deviations of hundreds of kiloparsecs from the orbit in the MW+LMC potential, suggesting it may be more perturbed by the SMC than the LMC. Tuc3 is another case where the SMC changes the long-term dynamics of a satellite even though the timing and distance at the most recent pericenter with respect to the MW and with to the LMC remain the same. Carefully

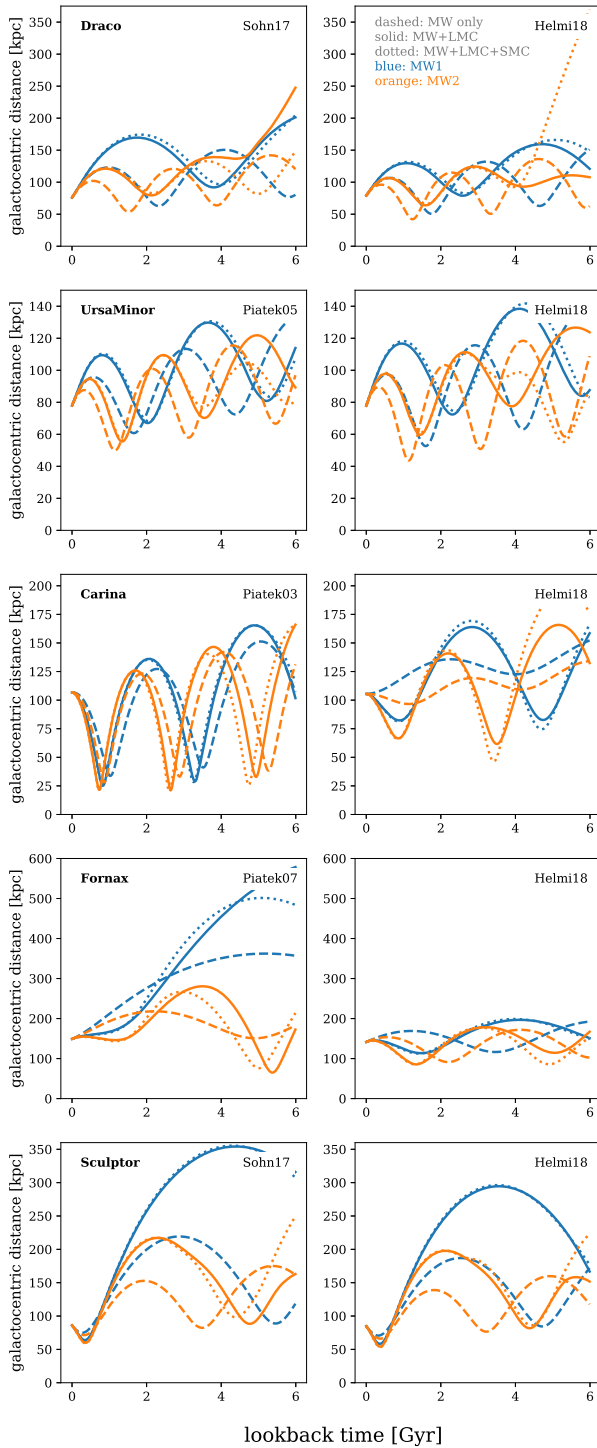


Figure 2. Direct orbits for the classical satellite galaxies included in our sample. The blue and orange lines indicate orbits calculated in MW1 and MW2, respectively. The left column shows direct orbits calculated using pre-*Gaia* DR2 PMs. The right column shows direct orbits calculated with *Gaia* DR2 PMs (see Tables 1 and 2.) All classical satellites are noticeably impacted by the addition of the LMC, regardless of the PM measurement used. Carina and Fornax exhibit significant changes in their orbits as a result of PM differences. The LMC impacts the dynamics of Carina, Fornax, and Sculptor most strongly, while the SMC does little to change the dynamics of the classical satellites.

determining which of the Clouds plays a more significant role in these satellite’s orbits requires further attention and is beyond the scope of this work.

4.3. Statistical Significance of Orbital Histories

As the direct orbits only represent one set of orbital solutions, we tabulate the average orbital properties across 1000 orbital calculations in the combined MW+LMC+SMC potential for each candidate Magellanic satellite. These orbits use Galactocentric positions and velocities derived from the Monte Carlo scheme discussed in Section 2 as initial conditions. Average orbital properties and corresponding standard errors are calculated with respect to the LMC and are listed in Table 7 (MW1) and Table 8 (MW2).

In each table Columns 1–8 list the fraction of 1000 orbits where the satellite reaches pericenter and apocenter (f_{peri} , f_{apo}), the fraction of orbits where the distance at pericenter is less than r_{outer} ($f_{r_{\text{outer}}}$, see Section 3.1.2 and Table 6), the distance of the most recent pericenter (r_{peri}) and apocenter (r_{apo}), and the time at which these occur on average (t_{peri} , t_{apo}). The second half of each table (Columns 9–16) lists the same quantities for the second pericenter and apocenter as a function of lookback time. Tables listing the orbital properties calculated with respect to LMC1 and LMC3 are provided in Appendices A and B. Orbital properties calculated with respect to the MW are provided in Appendix C.

4.4. Identifying Magellanic Satellites

To determine which of the candidate Magellanic satellites are true dynamical companions, we examine the orbital properties calculated relative to the fiducial LMC model. The left panel of Figure 4 illustrates r_{peri} versus the velocity at r_{peri} for the most recent pericentric passage in MW1. The average velocity and standard deviation is computed using only the subset of orbital solutions where $r_{\text{peri}} < r_{\text{outer}}$, denoted as $f_{r_{\text{outer}}}$ and indicated by the colorbar. The dashed blue line represents r_{outer} and the solid blue curve is the escape velocity of the fiducial LMC model. Using the properties shown in Figure 4, three criteria are defined to determine membership to the Magellanic system.

Criterion 1: First, we limit the sample of candidate satellites to only those galaxies whose orbits are dominated by the gravitational potential of the LMC rather than the MW’s for a high percentage of orbits. This is accomplished by selecting satellites with $f_{r_{\text{outer}}} > 0.5$, indicating that more than 50% of the PM error space allows for a closest approach within r_{outer} . By doing so, the following galaxies remain: Seg1, Tuc3, Scu1, Car2, Car3, Hor1, Hyi1, Ret2, and Phx2.

Criterion 2: Next, we examine which of the remaining candidate satellites have velocities that are comparable to or less than the escape velocity of the LMC. All candidate satellites whose velocities at r_{peri} fall below the blue solid curve (v_{esc} of the LMC) in Figure 4 remain. Seg1, Tuc3, and Scu1 have significantly higher velocities than the LMC’s escape speed. These galaxies are likely MW satellites that orbit within 50 kpc of the Galactic Center and consequently pass nearby the LMC. Additionally, all three satellites are especially unlikely to be companions of the LMC as they are on retrograde orbits compared to other satellites in the VPOS, including the MCs (Sohn et al. 2017; Fritz et al. 2018). We will refer to these galaxies as *MW satellites that recently interacted with the MCs*.

Our results for Tuc3’s orbit are well-aligned with recent literature wherein models of the formation of Tuc3’s stellar stream require a recent, close encounter with the LMC (Erkal et al. 2018; Li et al. 2018a; Simon 2018). This further suggests

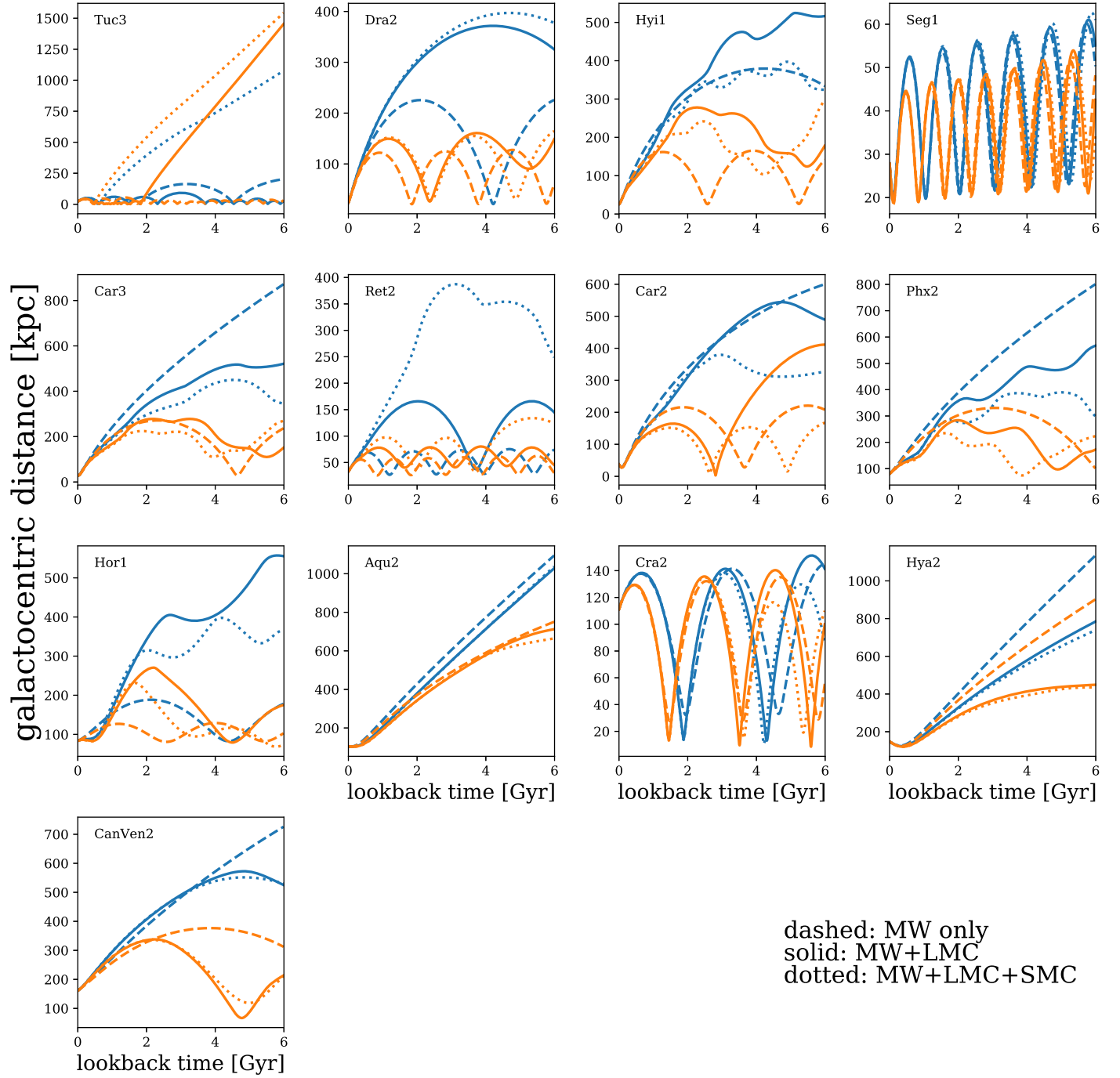


Figure 3. Direct orbits for all UFD satellite galaxies included in our sample. The blue lines indicate orbits calculated in MW1 while the orange lines represent MW2. Orbits are shown in the MW-only potential (dashed lines), the MW+LMC potential (solid lines), and the MW+LMC+SMC potential (dotted lines) using galactocentric quantities derived from *Gaia* DR2 PMs (see Tables 1 and 2). All satellites, with the exception of Seg1, Aqu2, Hya2, and CanVen2, are notably perturbed by the inclusion of the LMC. The addition of the SMC further perturbs the orbits of Hyi1, Car3, Ret2, Car2, Phx2, Tuc3 and Hor1. Of these, Tuc3 and Ret2 are the most highly affected, illustrating that the SMC can change the long-term dynamics of specific satellite’s orbits.

that Segue 1 may also have faint tidal debris resulting from a close passage with the LMC.

Criterion 3: Of the satellites that remain (Car2, Car3, Hor1, Hyi1, Phx2, Ret2), all six are to the left of the dashed blue line and below the solid blue line, indicating that they are bound to the LMC. Each satellite completes a recent passage around the LMC in the last 0.5 Gyr. To further separate these satellites into those that only recently passed around the LMC once versus those that may have completed multiple tightly bound orbits around the LMC, the right side of Figure 4 illustrates the same

quantities for the second to last pericentric passage. By applying Criterion 1 and Criterion 2 to the orbital properties at the second to last pericentric passage, Car2, Car3, Hor1, and Hyi1 remain. These satellites are therefore designated *long-term Magellanic satellites* since they complete two bound orbits on average around the LMC in the last 2.5–3 Gyr. The SMC, a long-term satellite, is also included in Figure 4 for reference. Ret2 and Phx2 are classified as *recently captured Magellanic satellites* since they only complete one bound orbit around the MCs in the last 1 Gyr.

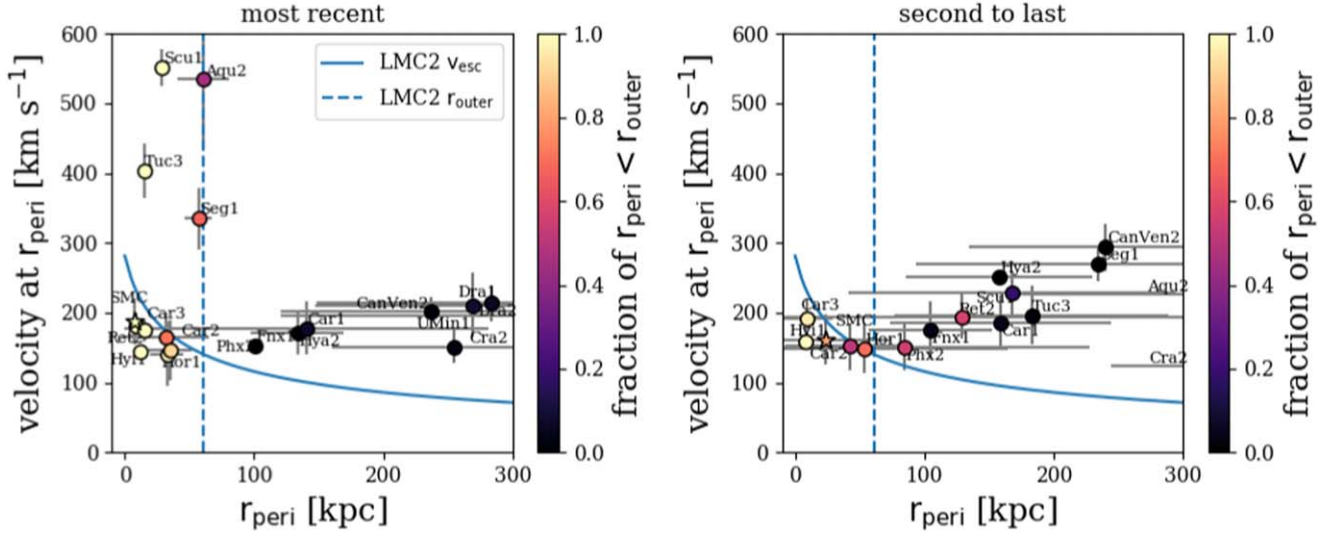


Figure 4. Distance at pericenter (r_{peri}) vs. the velocity at pericenter for the fraction of 1000 orbits where $r_{\text{peri}} < r_{\text{outer}}$ ($f_{\text{outer},1}$, indicated by the colorbar). All quantities are with respect to the LMC for the most recent passage (left) and the second to last passage around the LMC (right). These orbital parameters are calculated for MW1 and the fiducial LMC model (LMC2). The blue dashed line is r_{outer} for MW1 and LMC2. The solid blue curve represents the escape velocity curve for LMC2. Seg1, Tuc3, and Scu1 are all MW satellites that have recent encounters with the LMC. Ret2 and Phx2 are recently captured Magellanic satellites, while Car2, Car3, Hor1, and Hyi1 are long-term Magellanic satellites.

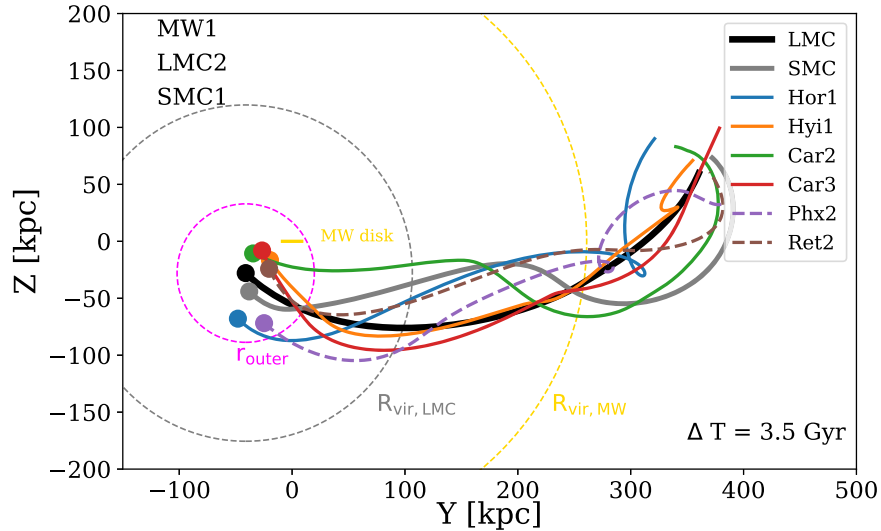


Figure 5. Direct orbits of all Magellanic satellites for the last 3.5 Gyr projected in the YZ-galactocentric plane. Recently captured Magellanic satellites (Ret2, Phx2) are illustrated with dashed lines and long-term Magellanic satellites (Car2, Car3, Hor1, Hyi1) are plotted with solid lines for MW1 using the fiducial LMC model. The disk of the MW lies along the z -axis. The orbit of the LMC (SMC) is illustrated in black (gray). The filled circles represent the positions of all satellites today. The magenta dashed circle indicates r_{outer} of the LMC and the gray dashed circle is the virial radius of the LMC. The gold dashed circle is the virial radius of the MW. The orbits of all Magellanic satellites follow the orbital path of the LMC.

For MW1 and the fiducial LMC, the orbits of these six Magellanic satellites are shown in Figure 5 along with the orbits of the LMC and the SMC for the last 3.5 Gyr. Orbits are plotted in the YZ-plane relative to the MW’s Galactic Center. The disk of the MW lies along the z -axis. The orbits of all Magellanic satellites clearly follow the orbital path of the LMC/SMC. A 3D animation showing the orbits of all 18 candidate Magellanic satellites using the MW1 and LMC2 models is available at <https://bit.ly/35wH5Tr>.

Figure 6 is the same as Figure 4 but for MW2 in the fiducial LMC model. Applying Criterion 1 and Criterion 2 to the left panel of Figure 6, we conclude that Seg1, Tuc3, and Scu1 are

still MW satellites that make a close passage around the LMC in the last 1 Gyr. Applying Criterion 3 to Figure 6, Ret2 and Phx2 are recently captured Magellanic satellites, while Car3, Hor1, Hyi1, and Phx2 are all long-term Magellanic satellite. Car2 now falls outside of the selection criteria due to an increase in r_{peri} by ~ 50 kpc in MW2. This is likely attributed to the difference in the LMC’s orbital history for MW1 and MW2. Satellites are less likely to remain members of the Magellanic system as the MCs pass around the MW two times in the last 6 Gyr (i.e., more severe tidal stripping owing to the MW in MW2 may yield fewer Magellanic satellites; see Sales et al. 2011). Note that the SMC is unbound from the LMC early in

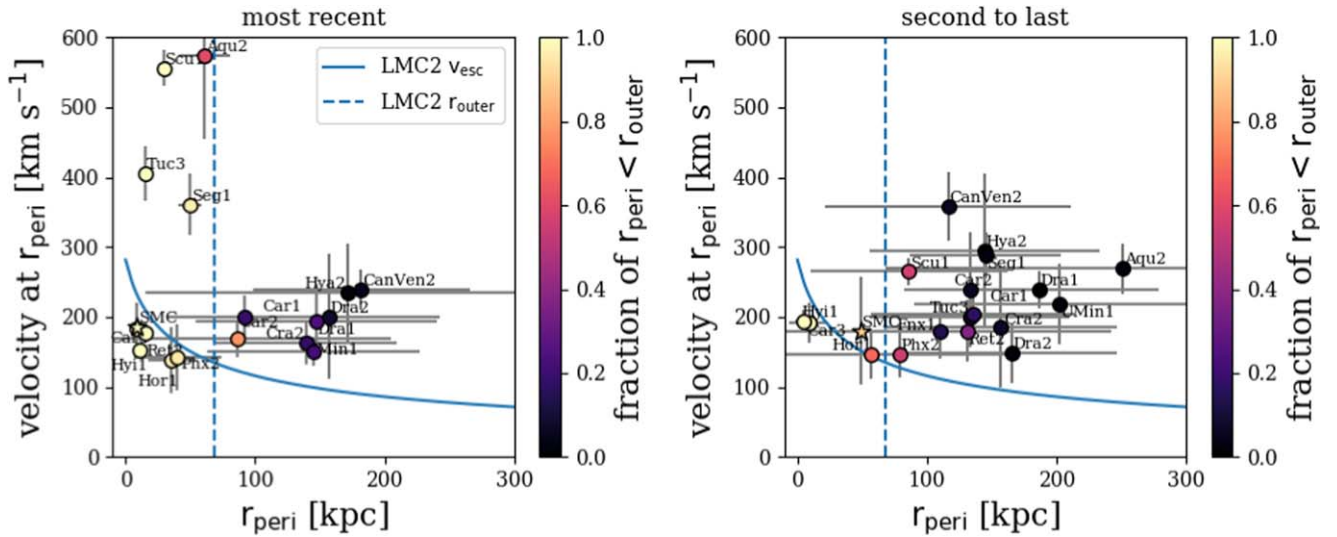


Figure 6. Same as Figure 4 except orbital parameters are calculated for MW2 and the fiducial LMC model (LMC2). Seg1, Tuc3, and Scu1 are all MW satellites that recently passed nearby the MCs at velocities well above the escape speed of the LMC. Ret2 and Phx2 are recently captured Magellanic satellites, while Car3, Hor1, and Hyi1 are long-term Magellanic satellites. In MW2, Car2 no longer qualifies as a satellite of the MCs.

MW2 as a high-mass MW cannot sustain a long-lived LMC–SMC binary (see Kallivayalil et al. 2013).

Table 9 provides a summary of candidate satellites separated into the classes identified above for all MW and LMC mass combinations. Analogous figures for LMC1 and LMC3 are provided in Appendices A and B, respectively.

The following galaxies are ruled out as Magellanic satellites: Car1, Dra1, UMin1, Fnx1, Cra2, CanVen2, Dra2, Hya2. While Aqu2, Tuc3, Seg1, and Scu1 can have close encounters with the LMC in specific MW–LMC mass combinations (see Table 9), we stress that they are not dynamically associated members of the Magellanic system. In Section 5.1, we compare these results to other recent studies and discuss how differing sets of selection criteria for identifying Magellanic satellites can lead to alternative conclusions.

5. Discussion

5.1. Comparison to Recent Literature

Here we will discuss our results in the context of a few recent studies on Magellanic satellites that are the most relevant to this analysis. Jethwa et al. (2016) derived probabilities for membership to the Magellanic system for 14 UFDs discovered in DES. Though PMs were not available at the time, they integrated orbits in a combined MW+LMC+SMC potential, including DF and tidal shredding. Satellites were initially radially distributed in a way that is consistent with cosmological simulations. Jethwa et al. (2016) found that seven UFDs have a high probability ($p > 0.7$) of being LMC satellites based on their positions (< 50 kpc from the LMC), and that of the four UFDs with measured velocities, these values are consistent with the LMC. The only overlapping satellites between our work and Jethwa et al. (2016) are Ret2 and Hor1, and both studies find that these satellites are highly likely satellites of the LMC.

Kallivayalil et al. (2018) compared the measured 3D kinematics of UFDs with the position and velocities of an LMC analog’s debris in a high-resolution simulation and concluded that Car2,

Car3, Hor1, and Hyi1 are all satellites that entered the MW’s halo with the MCs. They also found that Ret2 is not consistent with the kinematics of simulated LMC debris in all three velocity components, but its orbital pole is consistent with that of the debris, hinting at potential association.

Kallivayalil et al. (2018) indicated that Hya2 and Dra2 require more detailed orbital modeling, which we undertake in this paper. We find no association between these two galaxies and the MCs using our selection criteria. Our conclusions for satellite membership of four UFDs (Car2, Car3, Hyi1, Hor1) are consistent with Kallivayalil et al. (2018). Furthermore, the identification of recently captured Magellanic satellites in this work confirms the conclusion from Kallivayalil et al. (2018) that Ret2 is a tentative Magellanic satellite.

Pardy et al. (2020) used the Auriga simulations to count the abundance of satellites around LMC analogs and found that the LMC is expected to host ~ 3 satellites with $M_* \geq 10^5 M_\odot$ and within two times R_{200} of the LMC. The SMC counts toward this prediction and they additionally claimed that Carina and Fornax are also satellites of the LMC given the coherence between their orbital poles on the sky compared to that of the LMC. However, we do not find that Carina and Fornax are associated to the MCs using our satellite criteria, which accounts for the orbital histories of the galaxies in addition to their current kinematics and dynamics.

Jahn et al. (2019) used the subset of simulations from the FIRE suite hosting an LMC analog to calculate the expected abundance of LMC satellite galaxies and found that it can host 5–10 satellites with $M_* \geq 10^4 M_\odot$ within its virial radius. Like Pardy et al. (2020), they also used the recently measured PMs of UFDs and classical dwarfs to additionally quantify which of these galaxies have 3D angular momenta vectors that are consistent with the MCs, similar to the analysis of Sales et al. (2011, 2017). These authors concluded that given their current angular momenta, Car2, Car3, Hor1, Hyi1, Carina, and Fornax are all satellites of the LMC, in addition to the SMC. Using the satellite selection criteria defined in this work, we find good agreement with both Jahn et al. (2019) and Pardy et al. (2020)

Table 7
Orbital Properties with Respect to LMC2 in MW1

Name	$f_{\text{peri},1}$	$f_{\text{router},1}$	$r_{\text{peri},1}$ (kpc)	$t_{\text{peri},1}$ (Gyr)	$f_{\text{apo},1}$	$r_{\text{apo},1}$ (kpc)	$t_{\text{apo},1}$ (Gyr)
Most recent							
Aqu2	1.0	0.46	61.07 ± 20.0	0.16 ± 0.06	0.21	472.19 ± 160.67	3.07 ± 1.14
CanVen2	0.24	0.01	236.77 ± 115.85	3.38 ± 1.23	0.31	346.53 ± 115.15	1.88 ± 1.33
Car2	0.81	0.71	31.74 ± 33.71	1.24 ± 0.48	0.84	77.38 ± 81.01	0.66 ± 0.85
Car3	1.0	1.0	8.86 ± 3.08	0.18 ± 0.05	0.99	58.8 ± 42.4	1.0 ± 0.5
Cra2	1.0	0.04	254.33 ± 93.5	2.6 ± 0.82	1.0	348.69 ± 60.96	1.47 ± 0.33
Dra2	0.35	0.03	315.3 ± 195.24	4.41 ± 1.22	0.63	535.71 ± 151.29	3.13 ± 1.09
Hor1	0.98	0.97	32.59 ± 12.49	0.27 ± 0.32	0.92	140.61 ± 176.8	1.56 ± 1.42
Hyi1	1.0	1.0	11.81 ± 2.43	0.27 ± 0.04	1.0	30.3 ± 2.95	0.77 ± 0.08
Hya2	0.26	0.02	133.48 ± 36.1	0.86 ± 1.06	0.15	219.52 ± 120.46	1.02 ± 1.29
Phx2	0.97	0.91	34.75 ± 16.5	0.43 ± 0.4	0.89	181.56 ± 186.47	2.2 ± 1.3
Ret2	1.0	1.0	15.76 ± 2.92	0.12 ± 0.02	0.92	199.74 ± 217.83	1.91 ± 1.42
Seg1	0.99	0.67	56.84 ± 10.85	0.32 ± 0.11	0.99	70.17 ± 7.28	0.12 ± 0.04
Tuc3	1.0	1.0	14.82 ± 3.25	0.08 ± 0.01	0.72	219.89 ± 143.61	1.26 ± 1.05
Car1	0.68	0.08	140.66 ± 140.59	1.73 ± 1.33	0.93	280.58 ± 234.89	1.94 ± 1.81
Dra1	0.78	0.07	283.83 ± 135.04	4.27 ± 0.97	0.99	417.1 ± 86.54	2.43 ± 0.46
Fnx1	1.0	0.0	100.1 ± 4.52	0.14 ± 0.07	0.84	366.87 ± 259.49	2.88 ± 2.08
Scu1	1.0	1.0	28.91 ± 4.88	0.11 ± 0.01	0.83	338.49 ± 83.57	2.1 ± 0.75
UMin1	0.87	0.09	269.27 ± 122.35	3.78 ± 1.02	0.99	384.19 ± 63.84	2.13 ± 0.37
Name	$f_{\text{peri},2}$	$f_{\text{router},2}$	$r_{\text{peri},2}$ (kpc)	$t_{\text{peri},2}$ (Gyr)	$f_{\text{apo},2}$	$r_{\text{apo},2}$ (kpc)	$t_{\text{apo},2}$ (Gyr)
Second to last							
Aqu2	1.0	0.01	343.33 ± 181.56	4.23 ± 1.11	0.08	406.01 ± 149.01	4.82 ± 0.78
CanVen2	0.24	0.0	240.01 ± 105.2	4.51 ± 0.97	0.08	321.98 ± 109.63	4.58 ± 1.18
Car2	0.81	0.51	41.96 ± 49.18	4.03 ± 1.0	0.75	123.1 ± 94.32	3.08 ± 1.03
Car3	1.0	0.96	9.42 ± 19.26	1.75 ± 0.81	0.92	56.49 ± 23.13	2.45 ± 0.86
Cra2	1.0	0.0	431.89 ± 187.86	4.97 ± 0.69	0.88	426.21 ± 159.8	4.56 ± 0.65
Dra2	0.35	0.0	409.33 ± 163.4	5.1 ± 0.59	0.08	433.24 ± 152.79	4.95 ± 0.72
Hor1	0.98	0.7	53.75 ± 110.3	2.09 ± 1.37	0.69	73.3 ± 88.87	2.59 ± 1.21
Hyi1	1.0	1.0	8.4 ± 2.49	1.24 ± 0.14	1.0	28.95 ± 4.95	1.68 ± 0.21
Hya2	0.26	0.0	157.59 ± 71.85	5.05 ± 0.86	0.06	387.1 ± 165.66	4.14 ± 1.05
Phx2	0.97	0.56	84.1 ± 143.76	2.96 ± 1.26	0.57	103.64 ± 120.62	3.67 ± 1.1
Ret2	1.0	0.57	128.98 ± 199.41	2.46 ± 1.39	0.75	165.14 ± 206.47	3.07 ± 1.31
Seg1	0.99	0.0	234.4 ± 140.59	1.85 ± 1.1	0.98	261.92 ± 151.59	1.5 ± 1.03
Tuc3	1.0	0.03	182.68 ± 106.25	1.41 ± 1.17	0.55	298.44 ± 142.43	2.24 ± 1.37
Car1	0.68	0.05	158.4 ± 85.28	4.57 ± 0.97	0.52	272.18 ± 123.27	3.96 ± 1.01
Dra1	0.78	0.0	304.81 ± 0.0	4.58 ± 0.0	0.1	431.22 ± 221.96	5.56 ± 0.41
Fnx1	1.0	0.04	104.49 ± 47.78	1.7 ± 0.96	0.37	259.48 ± 88.69	4.07 ± 0.81
Scu1	1.0	0.18	167.35 ± 126.52	4.35 ± 0.85	0.2	256.8 ± 61.37	5.27 ± 0.57
UMin1	0.87	0.0	439.41 ± 237.89	4.87 ± 1.28	0.32	492.95 ± 201.59	5.5 ± 0.39

Note. Columns 1–8 refer to the most recent occurrence of a pericenter and apocenter. Columns 9–16 refer to the second to last instance where these minima and maxima occur. $f_{\text{peri},i}$ ($f_{\text{apo},i}$) is the fraction of 1000 orbits where a pericenter (apocenter) is recovered. (Every unique orbital solution does not result in the same number of apocenters and pericenters as a function of lookback time given the large PM uncertainties. Furthermore, some satellites on first infall never reach an apocenter within the last 6 Gyr.) $f_{\text{router},i}$ is the fraction of 1000 orbits with $r_{\text{peri}} < r_{\text{router}}$ (see Section 3.2.1).

in the ultrafaint regime, but we do not find that Carina and Fornax are dynamically associated Magellanic satellites even though their orbital poles are aligned today.

Erkal & Belokurov (2019) calculated the orbital energy of satellites 5 Gyr ago to determine whether they were energetically bound to the LMC. This process is repeated for 10,000 Monte Carlo realizations to derive a probability for being an LMC satellite as a function of LMC mass. In doing so, they found that Car2, Car3, Hor1, Hyi1, Phx2, and Ret2 are highly probable satellites of the LMC in addition to the SMC and that an LMC mass of $1.5 \times 10^{11} M_{\odot}$ is required for all to be bound simultaneously. In general, the results from Erkal & Belokurov (2019) are in good agreement with our fiducial LMC model.

Two main differences include that we find Car2 is not an LMC satellite in a high-mass MW model (MW2; see Section 5.2) and that Ret2 is only recently captured by the MCs in our categorization (i.e., it was not bound to the LMC 5 Gyr ago).

It is worth noting that each of the aforementioned analyses uses different criteria to select satellites that may be of Magellanic origin. We stress that even in our own analysis an alternative set of selection criteria may lead to different conclusions. For example, if we chose Magellanic satellites that satisfy $r_{\text{peri}} < R_{\text{vir,LMC}}$ instead of $r_{\text{peri}} < r_{\text{router}}$ and remove the escape velocity criteria in Section 4.4, a greater number of Magellanic satellites are identified. In particular, Carina and Fornax would be LMC satellites under these criteria, in line

Table 8
Orbital Properties with Respect to LMC2 in MW2

Name	$f_{\text{peri},1}$	$f_{\text{router},1}$	$r_{\text{peri},1}$ (kpc)	$t_{\text{peri},1}$ (Gyr)	$f_{\text{apo},1}$	$r_{\text{apo},1}$ (kpc)	$t_{\text{apo},1}$ (Gyr)
Most recent							
Aqu2	1.0	0.61	60.95 ± 19.87	0.16 ± 0.06	0.36	394.88 ± 171.75	2.1 ± 0.85
CanVen2	0.49	0.05	181.92 ± 83.48	2.33 ± 1.05	0.53	296.2 ± 102.69	1.08 ± 1.13
Car2	0.99	0.78	85.67 ± 118.73	1.54 ± 1.42	1.0	121.68 ± 139.86	0.93 ± 1.14
Car3	1.0	1.0	8.19 ± 3.1	0.18 ± 0.05	1.0	52.04 ± 36.9	0.86 ± 0.38
Cra2	1.0	0.18	139.11 ± 70.12	2.31 ± 0.61	1.0	270.27 ± 29.85	0.96 ± 0.13
Dra2	0.96	0.09	156.95 ± 85.75	3.25 ± 1.02	0.99	332.3 ± 107.4	1.56 ± 0.56
Hor1	0.97	0.97	35.68 ± 17.9	0.22 ± 0.38	0.97	125.39 ± 134.31	1.36 ± 1.33
Hyi1	1.0	1.0	11.1 ± 2.51	0.27 ± 0.03	1.0	35.12 ± 7.94	0.82 ± 0.16
Hya2	0.33	0.03	171.24 ± 155.53	1.27 ± 1.6	0.24	304.57 ± 215.14	1.56 ± 1.7
Phx2	0.97	0.95	40.15 ± 34.26	0.4 ± 0.54	0.95	165.11 ± 145.54	1.88 ± 1.24
Ret2	1.0	1.0	15.53 ± 3.01	0.13 ± 0.02	1.0	210.87 ± 122.79	1.78 ± 0.86
Seg1	1.0	0.96	49.9 ± 8.74	0.29 ± 0.08	1.0	69.35 ± 31.27	0.1 ± 0.17
Tuc3	1.0	1.0	15.15 ± 3.24	0.07 ± 0.01	0.85	171.86 ± 112.99	0.99 ± 0.84
Car1	0.96	0.19	91.19 ± 59.3	1.38 ± 0.93	1.0	145.07 ± 99.05	0.77 ± 0.76
Dra1	0.89	0.24	147.27 ± 93.11	3.77 ± 1.05	0.96	282.86 ± 47.45	1.78 ± 0.67
Fnx1	1.0	0.0	100.73 ± 3.88	0.12 ± 0.03	1.0	209.65 ± 157.71	1.39 ± 1.26
Scu1	1.0	1.0	29.2 ± 4.97	0.11 ± 0.01	1.0	232.14 ± 57.28	1.09 ± 0.32
UMin1	0.94	0.22	145.29 ± 82.16	3.42 ± 0.96	0.98	265.65 ± 36.64	1.55 ± 0.55
Name	$f_{\text{peri},2}$	$f_{\text{router},2}$	$r_{\text{peri},2}$ (kpc)	$t_{\text{peri},2}$ (Gyr)	$f_{\text{apo},2}$	$r_{\text{apo},2}$ (kpc)	$t_{\text{apo},2}$ (Gyr)
Second to last							
Aqu2	0.34	0.02	251.1 ± 183.45	3.46 ± 0.95	0.2	293.41 ± 120.06	4.18 ± 0.92
CanVen2	0.2	0.06	116.18 ± 95.01	4.72 ± 0.83	0.35	379.18 ± 183.57	4.07 ± 0.85
Car2	0.83	0.06	133.35 ± 50.7	4.02 ± 0.84	0.96	259.38 ± 97.27	3.21 ± 1.0
Car3	1.0	0.99	8.8 ± 15.23	1.52 ± 0.61	0.97	61.21 ± 44.92	2.32 ± 0.85
Cra2	0.82	0.08	157.11 ± 88.94	4.52 ± 0.91	0.92	245.66 ± 108.93	3.61 ± 0.74
Dra2	0.39	0.02	165.29 ± 80.87	4.74 ± 0.78	0.65	282.88 ± 104.43	4.3 ± 0.95
Hor1	0.86	0.68	56.87 ± 78.5	1.88 ± 1.42	0.77	98.65 ± 99.62	2.51 ± 1.31
Hyi1	1.0	1.0	4.42 ± 5.9	1.31 ± 0.27	1.0	38.32 ± 13.42	1.84 ± 0.33
Hya2	0.09	0.01	144.2 ± 88.82	4.45 ± 0.85	0.13	330.55 ± 129.64	3.42 ± 1.02
Phx2	0.84	0.56	78.44 ± 90.98	2.61 ± 1.23	0.68	138.36 ± 117.13	3.51 ± 1.2
Ret2	0.98	0.38	131.35 ± 110.18	2.68 ± 1.24	0.81	219.62 ± 138.69	3.26 ± 1.09
Seg1	1.0	0.03	145.19 ± 57.96	1.31 ± 0.55	1.0	176.33 ± 53.66	0.94 ± 0.37
Tuc3	0.83	0.1	133.46 ± 76.63	1.27 ± 0.97	0.74	224.04 ± 106.54	2.02 ± 1.21
Car1	0.75	0.17	135.55 ± 78.63	3.57 ± 1.02	0.85	195.61 ± 99.61	2.8 ± 0.99
Dra1	0.2	0.0	186.27 ± 91.85	5.29 ± 0.57	0.5	308.2 ± 152.04	4.68 ± 0.64
Fnx1	0.91	0.14	110.39 ± 53.27	2.03 ± 1.53	0.74	215.8 ± 83.4	2.88 ± 0.68
Scu1	1.0	0.56	85.93 ± 76.06	2.53 ± 0.5	0.99	271.3 ± 115.62	3.89 ± 0.7
UMin1	0.36	0.02	202.23 ± 112.33	5.23 ± 0.54	0.63	287.09 ± 151.25	4.42 ± 0.6

with the conclusions in Pardy et al. (2020), Jahn et al. (2019). These modified criteria would also falsely count the MW satellites that only recently interacted with the MCs once as Magellanic satellites.

5.2. Masses of the LMC and the MW

The identification of Magellanic satellites discussed in Section 4.4 and summarized in Table 9 is sensitive to both the mass of the LMC and the mass of the MW. For fixed LMC mass, but variable MW mass, results are usually the same. But, for fixed MW mass, and variable LMC mass, there are some notable differences.

For a fixed MW1 mass model, higher LMC masses tend toward more satellites classified as long-term Magellanic satellites since the LMC's gravity overcomes the MW's as the MW-LMC mass ratio decreases. For example, in LMC1 only Car3 and Hyi1 are long-term Magellanic satellites. LMC2 adds Car2 and Hor1, and furthermore for LMC3, Phx2 is additionally a long-term

Magellanic satellite. For all LMC mass models in MW1, Ret2 is always a recently captured Magellanic satellite. This suggests that Ret2 requires an even more massive LMC (i.e., $> 2.5 \times 10^{11} M_{\odot}$) for it to be bound to the MCs even though Erkal & Belokurov (2019) find that Ret2 needs the LMC's mass to be $\geq 9.5 \times 10^{10} M_{\odot}$ for it to be energetically bound.

In a similar fashion, increasing the LMC's mass leads to more MW satellites having recent interactions with the MCs. For LMC1, only Tuc3 and Scu1 pass Criteria 1 (see Section 4.4). For the fiducial LMC2 model, Seg1 is additionally an MW satellite that interacts with the MCs recently. Finally, for LMC3, Aqu2 also follows suit. Like Scu1, Tuc3, and Seg1, Aqu2 is also on a retrograde orbit relative to the LMC and other satellites in the VPOS.

For a fixed MW2 mass model, all results are the same as MW1 with the exception of Car2 for LMC2 and LMC3. This demonstrates that the mass of the LMC drives the classification, not the mass of the MW. Car2 is never a Magellanic satellite in MW2 as its distance at pericenter increases to

Table 9

Identification of Magellanic Satellites and Recent Encounters in an MW+LMC +SMC Potential

MW1	MW2
MW satellites, recent interaction with MCs	
LMC1	Tuc3, Scu1
LMC2	Seg1, Tuc3, Scu1
LMC3	Aqu2, Seg1, Tuc3, Scu1
Recently captured Magellanic satellites	
LMC1	Ret2
LMC2	Ret2, Phx2
LMC3	Ret2
Long-term Magellanic satellites	
LMC1	Car3, Hyi1
LMC2	Car2, Car3, Hor1, Hyi1
LMC3	Car2, Car3, Hor1, Hyi1, Phx2

Note. MW satellites, recent interaction with MCs: orbits where $f_{r_{\text{outer},1}} > 0.5$ and velocity at most recent $r_{\text{peri}} > v_{\text{esc,LMC}}$. Magellanic satellites, bound late: also have $f_{r_{\text{outer},1}} > 0.5$ and velocity at most recent pericenter $> v_{\text{esc,LMC}}$ (i.e., at least one bound orbit around the LMC). Magellanic satellites, bound early: Magellanic satellites that additionally satisfy the same set of criteria also for the second to last pericentric passage (i.e., at least two bound orbits around the LMC).

values beyond r_{outer} . This is in contrast to Erkal & Belokurov (2019) who find that Car2 requires a relatively low-mass LMC ($M = 2 \times 10^{10} M_{\odot}$) for it to be bound. However, there are several differences between our orbital model and that of Erkal & Belokurov (2019) that may account for this discrepancy, including: (1) the gravitational influence of the SMC, (2) the addition of a disk potential for the LMC, (3) modeling satellites as extended objects, and (4) implementing DF from both the MW and the LMC.

A low-mass MW (MW1) and massive LMC (LMC2, LMC3) are the most favorable for producing the highest total number of MW satellites with recent interactions with the MCs (four galaxies at maximum) and Magellanic satellites (six galaxies at maximum). This is due in large part to the LMC being on first infall and only making one passage around the MW recently, resulting in less tidal stripping of satellites. Second, a more massive LMC brings a greater number of satellites with it, as expected from hierarchical Λ CDM.

5.3. Inclusion of the SMC Potential

To understand how the inclusion of the SMC impacts our analysis of Magellanic satellites, we recalculate the orbital properties for all 18 galaxies in an MW+LMC gravitational potential, neglecting the SMC. Using these properties, we re-classify galaxies into the categories defined in Section 4.4 and present the results for all six MW–LMC mass combinations in Table 10.

When orbital properties are computed in an MW+LMC potential, we find nearly the same results for galaxies in the “MW satellites, recent interaction with the MCs” category. The only difference is that Aqu2 also interacts with the MCs in the MW2–LMC2 mass combination even though it is not identified as such when orbits are calculated in the MW+LMC+SMC potential. This suggests that the SMC may even perturb galaxies on first infall, retrograde orbits like Aqu2.

Table 10

Identification of Magellanic Satellites and Recent Encounters in an MW+LMC Potential (no SMC)

MW1	MW2
MW satellites, recent interaction with the MCs	
LMC1	Tuc3, Scu1
LMC2	Seg1, Tuc3, Scu1
LMC3	Aqu2, Seg1, Tuc3, Scu1
Recently captured Magellanic satellites	
LMC1	Ret2
LMC2	Hor1, Ret2, Phx2
LMC3	Phx2, Ret2
Long-term Magellanic satellites	
LMC1	Car3, Hyi1
LMC2	Car2, Car3, Hyi1
LMC3	Car2, Car3, Hor1, Hyi1

Overall, the total number of Magellanic satellite remains the same for the MW+LMC potential compared to the MW+LMC +SMC potential, and the same six satellites are always placed in the “long-term” and “recently captured” categories: Car2, Car3, Hor1, Hyi, Ret2, and Phx2. However, more UFDs are classified into the “recently captured” category in the MW–LMC potential.

The SMC can cause some generic changes to the average distance and timing of pericenter and apocenter. As a result, Ret2 and Phx2 are *always* recently captured by the MCs regardless of the MW and/or the LMC’s mass with no SMC. This is due to an increase in the distance at the second pericenter for both satellites, likely caused by the decreased mass of the combined MCs when the SMC is not included.

Similarly, Hyi1 and Hor1 are also occasionally recently captured Magellanic satellites, whereas they are always long-term Magellanic satellites for the combined MW+LMC+SMC potential. We conclude that the SMC’s gravitational influence changes the predicted longevity of satellites as Magellanic satellites, increasing the number of satellites that entered the MW’s halo with the MCs by one if the MCs are on first infall (i.e., the MW1 model). These results are consistent with Jethwa et al. (2016) who find that the inclusion of the SMC only impacts one of the UFDs they study.

We note that other MW satellites, such as the Sagittarius dSph, may also have had interactions with the MCs (e.g., Zhao 1998), potentially perturbing the orbits of the MCs and any satellites associated with them. However, investigating the influence of Sagittarius requires high-resolution N -body simulations that account for the mass-loss satellites experience as they repeatedly pass around the MW as well as the mass evolution of the MW and LMC, so we defer this to future work.

5.4. Effect of Reducing Proper Motion Uncertainty

PM uncertainties will decrease as the time baselines between *Gaia* data releases increases. Future PM measurements with *HST*+*James Webb Space Telescope* (*JWST*) will also yield higher-precision PMs for many of the galaxies included in our sample. For example, *JWST* ERS 1334 will yield an improved PM for Dra2 and *HST* GO-14734 will obtain first-epoch

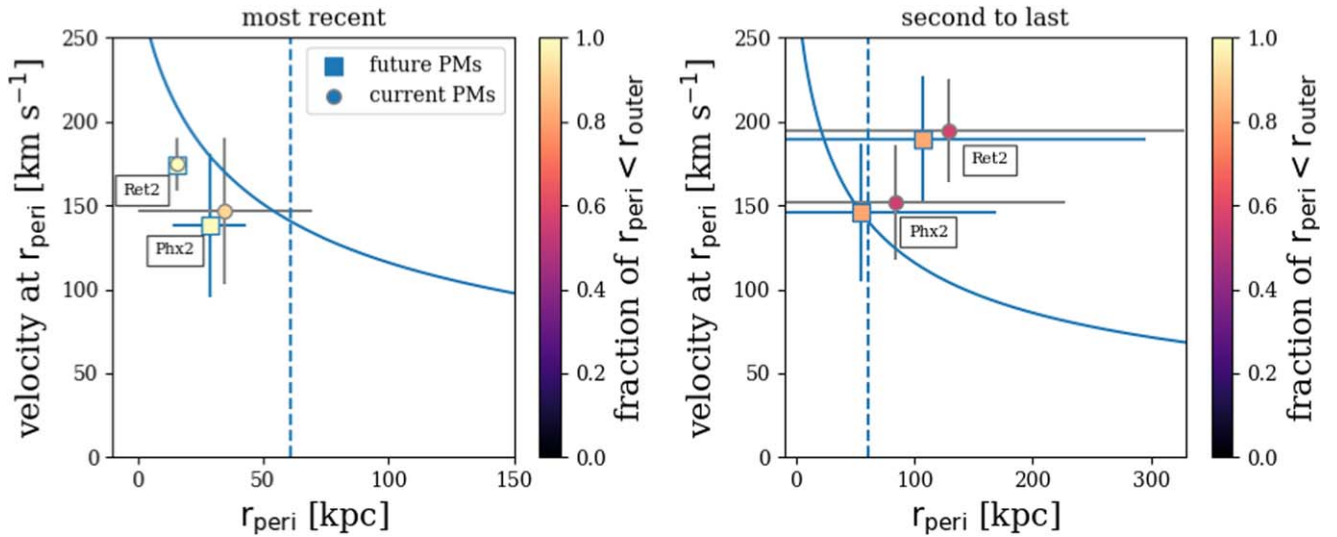


Figure 7. Distance and velocity at pericenter for Ret2 and Phx2 where filled circles and errors are identical to the data from Figure 4. Filled squares (future PMs) illustrate the same properties calculated when the measured uncertainty in PM components has been reduced to 25% of their current values. Smaller PM uncertainties decrease the distance and velocity at the most recent pericenter for Phx2 and yield similar average results, though with smaller error bars for Ret2. For the second pericentric passage, the distance at pericenter is reduced by ~ 20 kpc and the fraction of orbits where $r_{\text{peri}} < r_{\text{outer}}$ rises from 0.6 to 0.8 for both Ret2 and Phx2. A more precise PM measurement makes Phx2 a long-term Magellanic satellite, while Ret2 is still recently captured by the MCs.

imaging for eight galaxies in our sample that can be followed up with *JWST* to obtain improved PMs.

Given these future prospects, we recalculate the orbital properties of Ret2 and Phx2 after reducing the uncertainty in the *Gaia* DR2 PMs to 25% of their current values¹³ to determine how smaller PM uncertainties affect the identification of Magellanic satellites. We also set the PM covariance term to zero for this exercise.¹⁴ We focus on Ret2 and Phx2 because they are the only recently captured Magellanic satellites (see Section 4.4).

Figure 7 shows the resulting orbital properties for Ret2 and Phx2 when the PM uncertainties are reduced (filled squares) while keeping the most likely PM values fixed.¹⁵ The original values for the same properties are also plotted (filled circles) for reference. The orbital properties at the most recent pericenter (left panel) remain similar to the original results reported in Figure 4. At the second pericentric passage (right panel), more significant changes in r_{peri} and the fraction of orbits where $r_{\text{peri}} < r_{\text{outer}}$ are noticeable. There is a similar effect on both Ret2 and Phx2 in the right panel such that the average value of r_{peri} decreases by ~ 20 kpc and the fraction of satisfactory orbits increases to nearly 0.8 (see also Section 3 of Erkal & Belokurov 2019).

With smaller PM uncertainties, Phx2 becomes a long-term Magellanic satellite, while Ret2 remains a recently captured Magellanic satellite. However, it is yet to be determined whether this truly suggests Ret2 was only recently captured by the MCs or if this is an artifact of large uncertainties on orbital parameters even with smaller PM uncertainties. More precise

PM measurements are therefore necessary to confirm or invalidate their short-lived nature as Magellanic satellites.

6. Conclusions

We have used *Gaia* DR2 PMs to calculate the orbital histories of 13 UFD galaxies and five classical dwarf spheroidals within the VPOS to identify which galaxies are the most likely to be Magellanic satellites. These orbits are computed in a static MW+LMC+SMC potential where all galaxies, including the MW, are free to move in response to the gravitational influence of each other. DF from the MW and LMC are also included where the latter is calibrated to a realistic SMC orbit from *N*-body simulations.

We also calculate orbits in an MW-only and MW+LMC potential for comparison. Orbits are calculated for both a low-mass MW1 ($M_{\text{vir}} = 10^{12} M_{\odot}$) and high-mass MW2 ($M_{\text{vir}} = 1.5 \times 10^{12} M_{\odot}$) potential as well as three different LMC mass models ($M_{\text{vir}} = 0.8, 1.8, 2.5 \times 10^{11} M_{\odot}$). Our findings are summarized below:

1. Direct orbital histories for all 18 galaxies in our sample using the fiducial LMC model (LMC2) are presented in Figures 2 and 3. These orbits represent one orbital solution calculated from the average PM, line-of-sight velocity, and distance modulus converted to Galactocentric quantities. For the classical dwarfs, direct orbits using both previously measured PMs and *Gaia* DR2 PMs are calculated. We find consistency for all satellites except Fornax, which completes multiple passages around the MW at closer distances than predicted by previous PMs. The orbits of all five classical satellites are noticeably impacted by the inclusion of the LMC. These differences manifest as changes in the orbital period, distance at pericenter and apocenter, as well as the timing of these critical points. The SMC has a less significant effect on the orbits of classical dwarfs.

¹³ For *Gaia*, this roughly corresponds to a 7 yr baseline between DR1 and the final data release, so it is possible to reach this precision in the next decade.

¹⁴ We have checked that setting the PM covariance to zero with the current PM values does not significantly affect the average and standard errors on orbital properties reported in Section 4.3 for a fair comparison.

¹⁵ In reality, the most likely value for both PM components will also shift by $\sim 1\sigma$ on average, further increasing the chances that satellites will be reclassified from one category to another.

2. The gravitational influence of the LMC and SMC each impact the direct orbits of the UFD satellites. The SMC has a more noticeable effect compared to the orbits of the classical dwarfs, such that it too can alter the timing and distances at pericenter and apocenter. The LMC most significantly perturbs the direct orbits of the following UFD satellites: Car2, Car3, Hor1, Hyi1, Ret2, Tuc3, and Phx2. The addition of SMC in particular highly affects the orbits and long-term dynamics of Tuc3 and Ret2.
3. By evaluating the statistical significance of orbital properties calculated relative to the LMC in a combined LMC+SMC+MW potential, we separate galaxies into the following classes: (1) long-term Magellanic satellites, (2) recently captured Magellanic satellites, (3) MW satellites that have recently interacted with the MCs, and (4) MW satellites. For the fiducial LMC model (LMC2), Car2, Car3, Hor1, and Hyi1 are identified as long-term satellites, while Ret2 and Phx2 are recently captured Magellanic satellites (see Table 9).
4. The masses of the MW and LMC play key roles in the classification of Magellanic satellites. In a low-mass MW (MW1), the LMC is on first infall only completing one recent passage around the MW, whereas for a high-mass MW, the LMC completes two pericentric passages in the last 6 Gyr. The binarity of the LMC–SMC orbit is also short-lived for MW2. As a result, the highest number of Magellanic satellites are identified for a low-mass MW (MW1) and high-mass LMC (LMC2, LMC3) combination. Results are similar between MW1 and MW2 except that Car2 is not a Magellanic satellite for a high-mass MW (MW2).
5. In Table 10, we tabulate the impact of the SMC’s gravitational influence on the orbital histories of galaxies in our sample. By calculating the statistical significance of orbital properties in an MW+LMC potential (no SMC), we find the same total number of Magellanic satellites but with a larger fraction that are recently captured by the MCs. This suggests that the SMC impacts the implied longevity of Magellanic satellites. Ret2 and Phx2 are exclusively identified as recently captured Magellanic satellites in the MW+LMC potential, whereas they can be long-term Magellanic satellites in the MW+LMC+SMC potential. Hor1 and Hyi1 are also categorized as recently captured Magellanic satellites in certain MW–LMC mass combinations, but are always long-term Magellanic satellites in the MW+LMC+SMC scenario.
6. PMs will become more precise as upcoming measurements from *Gaia*, *HST*, and *JWST* are taken with longer time baselines between epochs. We tested whether reducing the PM measurement errors of Ret2 and Phx2 to 25% of their current values provides more narrow constraints on their orbital histories. Ret2 is still always recently captured by the MCs, but Phx2 can be a long-term Magellanic satellite with smaller PM uncertainties. However, improved PMs are necessary to determine whether our results for recently captured Magellanic satellites are truly short-lived members of the Magellanic system or if this is an artifact of large orbital uncertainties.

Our findings that a total of 3–6 of the 18 galaxies analyzed in this work are identified as Magellanic satellites are consistent with the

low end of cosmological expectations (e.g., Sales et al. 2013, 2017; Deason et al. 2015; Dooley et al. 2017; Jahn et al. 2019). The recent findings of Nadler et al. (2019) are most applicable to our analysis as they account for the survey footprints in which our sample of UFDs were discovered. These authors use an observational selection function combined with theoretical models to determine that 4.7 ± 1.8 satellites observed with DES and PS1 are LMC-associated satellites. In Nadler et al. (2019), *LMC-associated* refers to surviving satellites residing within the LMC’s virial radius at the time the LMC falls into the MW’s halo (which they find is ≤ 2 Gyr ago). While our definition of Magellanic satellites differs from that of Nadler et al. (2019), the consistency between our results is promising.

Varying criteria have recently been used to identify Magellanic satellites, leading to a wide range of conclusions for the same galaxies. A common definition for identifying satellites around complex systems such as the MCs is therefore necessary both in cosmological studies and in studies like this that use astrometry and orbital histories to determine membership. If UFDs are detected around M33 in the near future, as predicted in Patel et al. (2018), and PMs are obtained in the decade to follow, this will be crucial for determining whether these satellites are dynamically associated to M33 or M31.

Chemical abundance measurements and forthcoming star formation histories (SFHs) will both play key roles in identifying observational trends that complement the orbital histories of Magellanic satellites presented in this work. Chemical abundance ratios provide one opportunity for uncovering the formation histories of UFDs, and these signatures may provide an independent method of separating Magellanic UFDs from MW UFDs. Detailed chemical abundance analyses have been carried out for four of our Magellanic satellites (Ji et al. 2016; Nagasawa et al. 2018; Ji et al. 2019). However, more analysis is necessary to conclusively state whether there are obvious differences between Magellanic and MW UFDs.

SFHs are only available for two of the UFD satellites in our sample (Brown et al. 2014; Weisz et al. 2014). Upcoming SFHs of Magellanic satellites derived from deep *HST* imaging (*HST* program GO-14734; P.I.—N. Kallivayalil) will specifically illuminate differences between SFHs of the UFDs that are of Magellanic origin and those that are purely satellites of the MW (E. Sacchi et al. 2020, in preparation).

E.P. was supported by the National Science Foundation through the Graduate Research Fellowship Program funded by grant award No. DGE-1746060 and is currently supported by the Miller Institute for Basic Research, University of California Berkeley. N.K. is supported by NSF CAREER award 1455260. G.B. acknowledges support from NSF Grant AST-1714979. N. G.C. is supported by NASA 17-ATP17-0006 and HST-AR-15004. D.R.W. acknowledges fellowship support from the Alfred P. Sloan Foundation and the Alexander von Humboldt Foundation. This support was provided by NASA through grant numbers HST-GO-15476 and JWST-DD-ERS-1334 from the Space Telescope Science Institute, which is operated by AURA, Inc., under NASA contract NAS5-26555. M.B.K. acknowledges support from NSF CAREER award AST-1752913, NSF grant AST-1910346, NASA grant NNX17AG29G, and HST-AR-14282, HST-AR-14554, HST-AR-15006, HST-GO-14191, and HST-GO-15658 from STScI. F.A.G. acknowledges financial support from CONICYT through the project FONDECYT

Regular Nr. 1181264, and funding from the Max Planck Society through a Partner Group grant. E.P. would like to thank Rachel Smullen for stimulating discussions that have improved the quality of this work. The authors would also like to thank the referee for their helpful comments.

Software: astropy (The Astropy Collaboration et al. 2018), matplotlib (Hunter 2007), numpy (van der Walt et al. 2011), and scipy (Jones et al. 2001).

Appendix A

Results of Orbital Parameters for LMC1

Figures A1 and A2 show the resulting orbital properties of all candidate Magellanic satellites calculated with respect to LMC1. Figure A1 shows the results using LMC1 for MW1 and Figure A2 shows the results using LMC1 and MW2. Tables A1 (MW1) and A2 (MW2) list the orbital properties of all galaxies using LMC1 and each MW mass model.

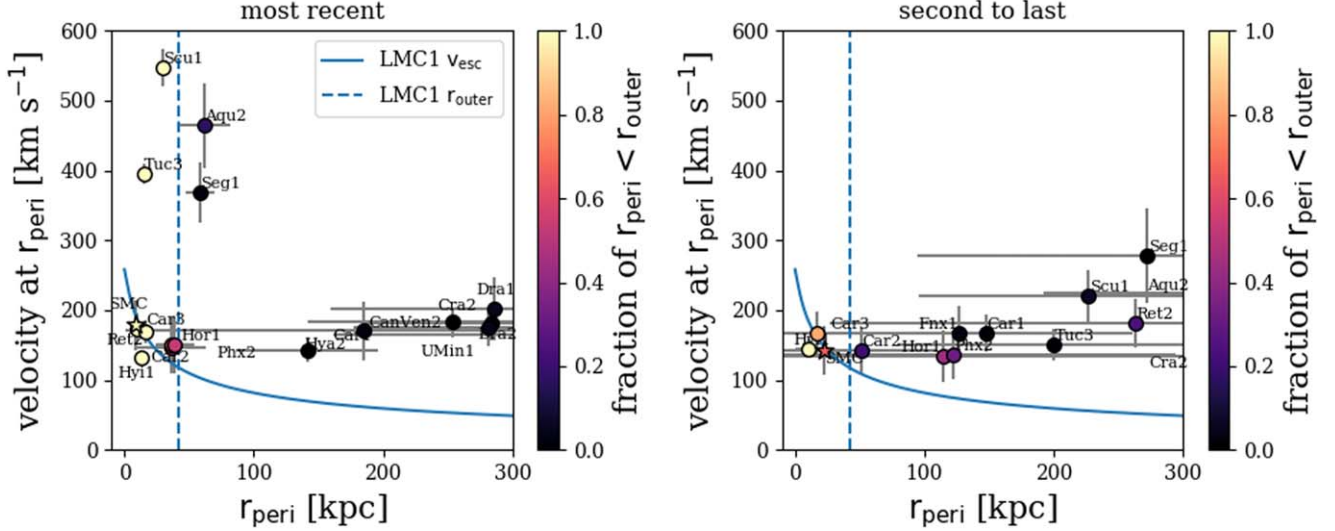


Figure A1. Same as Figure 4 except the orbital properties are calculated relative to LMC1 in MW1.

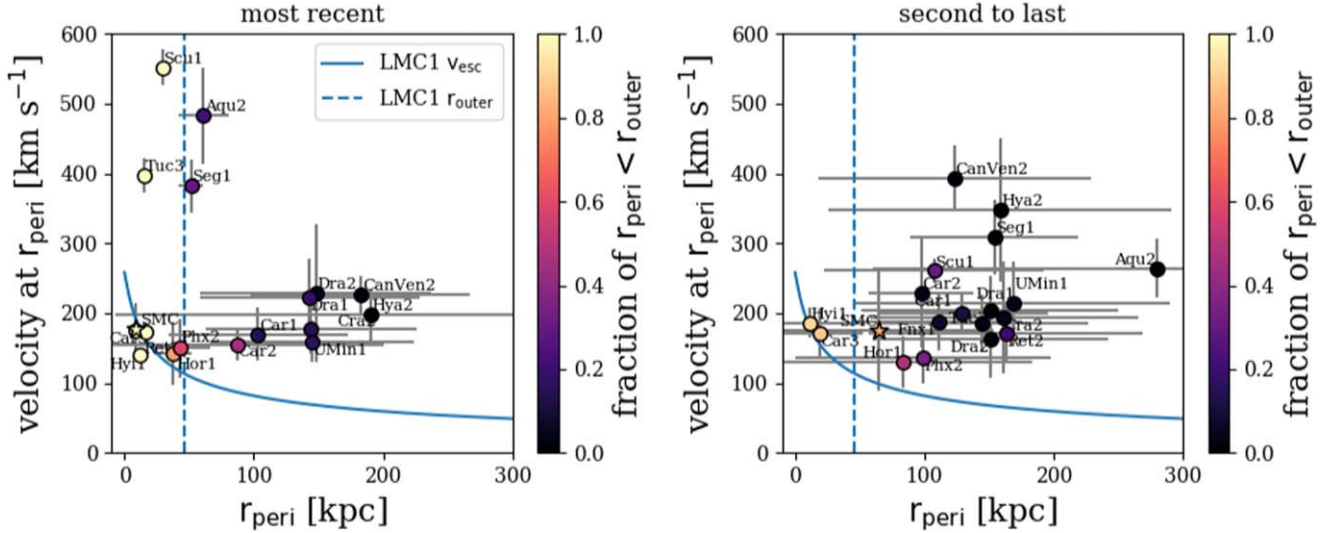


Figure A2. Same as Figure 4 except the orbital properties are calculated relative to LMC1 in MW2.

Table A1
Orbital Properties with Respect to the LMC in MW1 Using the LMC1 Model

Name	$f_{\text{peri},1}$	$f_{r_{\text{outer}},1}$	$r_{\text{peri},1}$ (kpc)	$t_{\text{peri},1}$ (Gyr)	$f_{\text{apo},1}$	$r_{\text{apo},1}$ (kpc)	$t_{\text{apo},1}$ (Gyr)
Most recent							
Aqu2	1.0	0.17	61.35 \pm 19.88	0.16 \pm 0.06	0.21	524.34 \pm 183.63	3.29 \pm 1.2
CanVen2	0.22	0.0	254.13 \pm 112.56	3.46 \pm 1.12	0.27	346.95 \pm 116.69	1.84 \pm 1.21
Car2	0.7	0.46	35.76 \pm 26.65	1.61 \pm 0.45	0.72	82.93 \pm 76.63	0.8 \pm 0.83
Car3	1.0	1.0	9.21 \pm 3.35	0.19 \pm 0.06	0.92	79.16 \pm 75.02	1.5 \pm 0.87
Cra2	1.0	0.02	283.37 \pm 96.07	2.38 \pm 0.68	1.0	358.54 \pm 72.79	1.51 \pm 0.38
Dra2	0.43	0.0	343.9 \pm 181.82	4.05 \pm 1.21	0.69	549.2 \pm 165.28	3.07 \pm 1.16
Hor1	0.96	0.68	35.74 \pm 11.27	0.2 \pm 0.31	0.84	211.45 \pm 228.29	2.01 \pm 1.66
Hyi1	1.0	1.0	12.98 \pm 2.75	0.29 \pm 0.05	1.0	34.66 \pm 10.9	0.99 \pm 0.27
Hya2	0.25	0.0	141.1 \pm 54.5	0.81 \pm 1.03	0.13	207.28 \pm 95.15	0.84 \pm 1.01
Phx2	0.96	0.53	38.7 \pm 14.94	0.35 \pm 0.3	0.75	235.18 \pm 217.07	2.56 \pm 1.42
Ret2	1.0	1.0	16.23 \pm 2.88	0.12 \pm 0.02	0.86	339.18 \pm 232.4	2.8 \pm 1.41
Seg1	0.99	0.03	58.43 \pm 11.07	0.31 \pm 0.1	0.99	70.39 \pm 7.3	0.12 \pm 0.05
Tuc3	1.0	1.0	14.87 \pm 3.22	0.08 \pm 0.0	0.8	222.0 \pm 142.07	1.2 \pm 1.0
Car1	0.58	0.03	184.45 \pm 183.38	2.18 \pm 1.59	0.88	356.52 \pm 266.38	2.46 \pm 1.9
Dra1	0.95	0.06	285.94 \pm 126.55	3.7 \pm 0.92	1.0	393.89 \pm 79.58	2.11 \pm 0.38
Fnx1	1.0	0.0	100.4 \pm 3.92	0.13 \pm 0.03	0.78	432.72 \pm 282.78	3.26 \pm 2.07
Scu1	1.0	0.99	29.13 \pm 4.9	0.11 \pm 0.01	0.76	351.74 \pm 79.49	2.1 \pm 0.66
UMin1	0.97	0.04	281.14 \pm 103.66	3.18 \pm 0.89	0.99	361.69 \pm 58.79	1.86 \pm 0.29
Name	$f_{\text{peri},2}$	$f_{r_{\text{outer}},2}$	$r_{\text{peri},2}$ (kpc)	$t_{\text{peri},2}$ (Gyr)	$f_{\text{apo},2}$	$r_{\text{apo},2}$ (kpc)	$t_{\text{apo},2}$ (Gyr)
Second to last							
Aqu2	1.0	0.0	384.45 \pm 192.93	4.22 \pm 1.15	0.07	426.56 \pm 167.58	4.83 \pm 0.82
CanVen2	0.22	0.0	214.71 \pm 160.25	4.76 \pm 0.64	0.05	369.94 \pm 124.55	4.81 \pm 0.83
Car2	0.7	0.21	51.12 \pm 58.67	4.63 \pm 0.88	0.54	141.03 \pm 107.07	3.92 \pm 1.04
Car3	1.0	0.82	16.4 \pm 30.76	2.53 \pm 1.13	0.69	66.18 \pm 32.89	3.34 \pm 1.1
Cra2	1.0	0.0	497.01 \pm 188.07	5.05 \pm 0.63	0.92	485.06 \pm 177.36	4.48 \pm 0.6
Dra2	0.43	0.0	421.15 \pm 178.1	5.06 \pm 0.78	0.1	436.93 \pm 139.38	4.78 \pm 0.8
Hor1	0.96	0.44	113.94 \pm 185.17	2.49 \pm 1.61	0.51	101.38 \pm 140.55	3.07 \pm 1.21
Hyi1	1.0	0.99	10.2 \pm 9.79	1.64 \pm 0.36	0.99	35.57 \pm 17.28	2.28 \pm 0.53
Hya2	0.25	0.0	182.77 \pm 116.04	4.94 \pm 1.09	0.04	422.79 \pm 178.87	4.32 \pm 0.98
Phx2	0.96	0.32	122.39 \pm 172.24	3.35 \pm 1.37	0.37	146.0 \pm 184.07	4.04 \pm 1.06
Ret2	1.0	0.24	262.55 \pm 235.88	3.31 \pm 1.36	0.54	325.57 \pm 259.65	4.01 \pm 1.14
Seg1	0.99	0.0	271.96 \pm 177.62	2.01 \pm 1.25	0.97	300.59 \pm 189.41	1.71 \pm 1.23
Tuc3	1.0	0.01	199.72 \pm 121.01	1.33 \pm 1.12	0.61	325.56 \pm 139.88	2.15 \pm 1.18
Car1	0.58	0.02	147.17 \pm 61.4	5.01 \pm 0.65	0.43	307.5 \pm 125.57	4.25 \pm 0.84
Dra1	0.95	0.0	272.23 \pm 297.87	5.92 \pm 0.03	0.27	466.2 \pm 195.48	5.54 \pm 0.34
Fnx1	1.0	0.03	127.04 \pm 133.85	2.01 \pm 1.07	0.27	297.93 \pm 102.75	4.47 \pm 0.8
Scu1	1.0	0.07	226.53 \pm 131.15	4.14 \pm 0.78	0.19	286.11 \pm 118.52	5.34 \pm 0.49
UMin1	0.97	0.0	470.22 \pm 293.96	5.74 \pm 0.27	0.58	515.69 \pm 186.78	5.36 \pm 0.37

Table A2
Orbital Properties with Respect to the LMC in MW2 Using the LMC1 Model

Name	$f_{\text{peri},1}$	$f_{\text{router},1}$	$r_{\text{peri},1}$ (kpc)	$t_{\text{peri},1}$ (Gyr)	$f_{\text{apo},1}$	$r_{\text{apo},1}$ (kpc)	$t_{\text{apo},1}$ (Gyr)
Most recent							
Aqu2	1.0	0.22	61.23 ± 19.75	0.16 ± 0.06	0.37	438.95 ± 209.94	2.26 ± 0.96
CanVen2	0.46	0.02	182.51 ± 84.93	2.43 ± 1.05	0.5	298.37 ± 95.93	1.1 ± 1.11
Car2	0.96	0.46	87.01 ± 113.4	2.1 ± 1.77	0.99	156.82 ± 160.13	1.31 ± 1.39
Car3	1.0	1.0	8.48 ± 3.37	0.19 ± 0.05	0.99	70.29 ± 69.51	1.19 ± 0.64
Cra2	1.0	0.15	143.9 ± 81.43	2.31 ± 0.66	1.0	274.55 ± 29.7	0.98 ± 0.13
Dra2	0.97	0.05	147.78 ± 89.45	3.08 ± 1.03	1.0	331.39 ± 107.22	1.5 ± 0.56
Hor1	0.96	0.79	37.61 ± 14.73	0.15 ± 0.29	0.94	169.88 ± 156.07	1.66 ± 1.47
Hyi1	1.0	1.0	12.1 ± 2.88	0.29 ± 0.04	0.99	55.09 ± 78.57	1.21 ± 0.84
Hya2	0.32	0.01	190.36 ± 197.45	1.22 ± 1.49	0.22	311.38 ± 237.37	1.48 ± 1.66
Phx2	0.96	0.59	42.57 ± 23.21	0.32 ± 0.46	0.92	207.1 ± 155.49	2.15 ± 1.24
Ret2	1.0	1.0	15.99 ± 2.98	0.12 ± 0.02	1.0	247.06 ± 98.47	1.89 ± 0.7
Seg1	1.0	0.3	51.31 ± 8.97	0.29 ± 0.08	1.0	69.63 ± 33.66	0.1 ± 0.18
Tuc3	1.0	1.0	15.23 ± 3.24	0.07 ± 0.01	0.92	178.01 ± 117.92	0.99 ± 0.83
Car1	0.95	0.15	103.28 ± 69.42	1.6 ± 1.14	1.0	164.79 ± 121.2	0.92 ± 0.9
Dra1	0.98	0.18	142.83 ± 84.75	3.3 ± 0.79	1.0	265.79 ± 43.83	1.5 ± 0.38
Fnx1	1.0	0.0	100.91 ± 3.83	0.12 ± 0.02	1.0	232.67 ± 174.02	1.57 ± 1.34
Scu1	1.0	1.0	29.41 ± 4.98	0.11 ± 0.01	1.0	245.7 ± 66.0	1.14 ± 0.37
UMin1	1.0	0.16	145.05 ± 78.86	2.93 ± 0.77	1.0	250.34 ± 34.49	1.31 ± 0.25
Name	$f_{\text{peri},2}$	$f_{\text{router},2}$	$r_{\text{peri},2}$ (kpc)	$t_{\text{peri},2}$ (Gyr)	$f_{\text{apo},2}$	$r_{\text{apo},2}$ (kpc)	$t_{\text{apo},2}$ (Gyr)
Second to last							
Aqu2	0.34	0.01	279.96 ± 220.34	3.56 ± 0.98	0.2	300.61 ± 131.26	4.14 ± 0.93
CanVen2	0.19	0.03	123.0 ± 105.32	4.72 ± 0.87	0.32	364.42 ± 167.03	4.07 ± 0.87
Car2	0.69	0.04	97.3 ± 40.28	4.24 ± 0.79	0.8	231.47 ± 81.47	3.31 ± 0.96
Car3	0.98	0.88	18.55 ± 33.67	2.08 ± 0.86	0.86	75.49 ± 52.52	3.03 ± 0.98
Cra2	0.82	0.05	161.3 ± 103.94	4.55 ± 0.85	0.92	250.7 ± 113.17	3.57 ± 0.73
Dra2	0.54	0.02	150.79 ± 90.67	4.66 ± 0.8	0.76	268.73 ± 113.84	4.11 ± 0.98
Hor1	0.83	0.48	83.9 ± 99.42	2.31 ± 1.56	0.71	134.67 ± 121.64	3.2 ± 1.45
Hyi1	0.95	0.92	11.04 ± 43.81	1.74 ± 0.64	0.93	52.09 ± 40.77	2.49 ± 0.64
Hya2	0.08	0.01	158.48 ± 132.38	4.58 ± 0.79	0.12	346.04 ± 135.04	3.63 ± 0.98
Phx2	0.8	0.35	99.07 ± 98.97	3.05 ± 1.3	0.57	167.55 ± 127.39	3.94 ± 1.17
Ret2	0.99	0.2	162.81 ± 105.67	2.81 ± 1.01	0.81	270.79 ± 127.19	3.52 ± 1.04
Seg1	1.0	0.02	153.9 ± 64.95	1.35 ± 0.6	1.0	184.04 ± 59.57	0.97 ± 0.4
Tuc3	0.9	0.04	144.94 ± 81.32	1.23 ± 0.97	0.84	237.69 ± 111.76	1.98 ± 1.22
Car1	0.8	0.11	129.35 ± 65.79	4.02 ± 0.85	0.89	213.08 ± 101.54	2.95 ± 0.85
Dra1	0.39	0.02	150.86 ± 99.2	5.23 ± 0.52	0.73	295.67 ± 160.63	4.4 ± 0.59
Fnx1	0.88	0.08	110.86 ± 64.79	2.22 ± 1.54	0.7	234.46 ± 87.11	3.1 ± 0.7
Scu1	0.99	0.31	107.34 ± 85.09	2.54 ± 0.43	0.99	282.18 ± 144.25	3.83 ± 0.64
UMin1	0.64	0.05	168.6 ± 121.31	5.08 ± 0.52	0.85	276.28 ± 153.26	4.08 ± 0.54

Appendix B

Results of Orbital Parameters for LMC3

Figures B1 and B2 show the resulting orbital properties of all candidate Magellanic satellites calculated with respect to

LMC3. Figure B1 shows the results using LMC3 for MW1 and Figure B2 shows the results using LMC3 and MW2. Tables B1 (MW1) and B2 (MW2) list the orbital properties of all galaxies using LMC3 and each MW mass model.

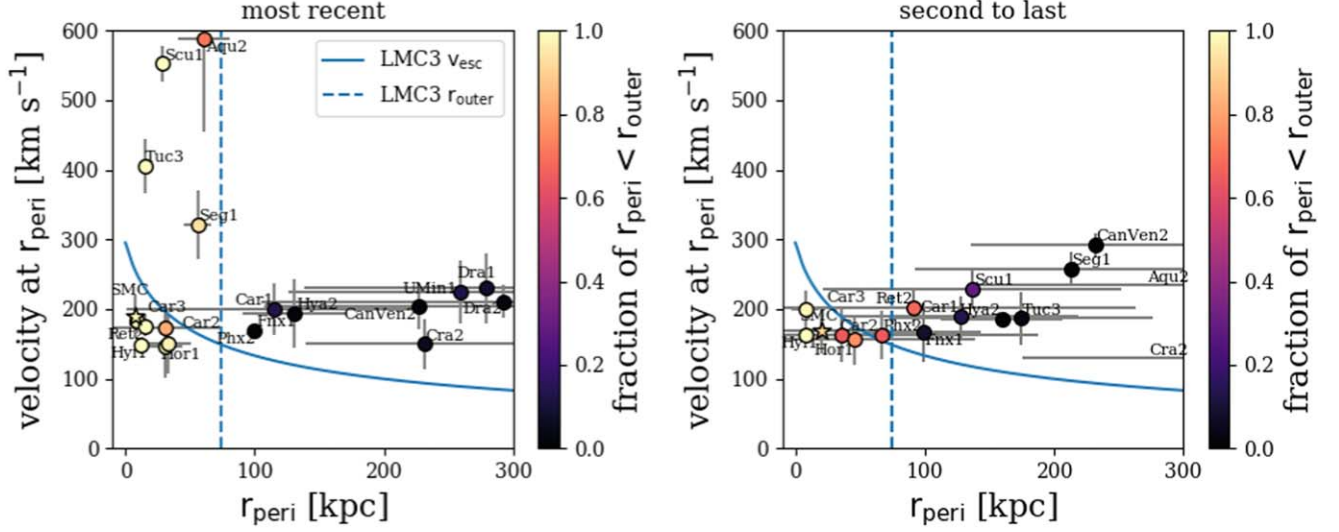


Figure B1. Same as Figure 4 except the orbital properties are calculated relative to LMC3 in MW1.

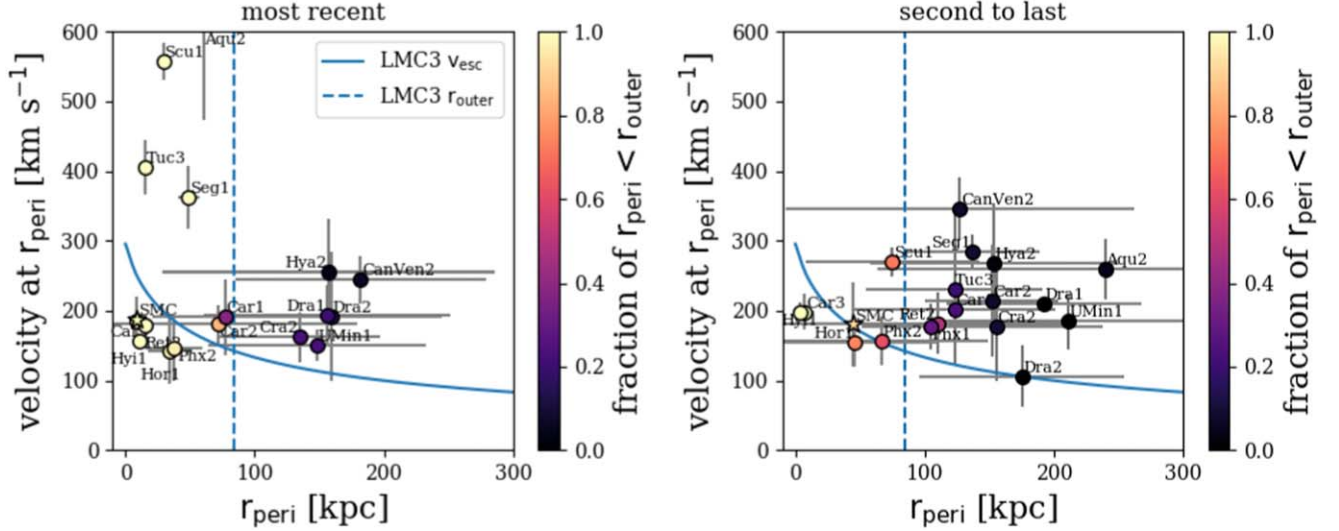


Figure B2. Same as Figure 4 except the orbital properties are calculated relative to LMC3 in MW2.

Table B1
Orbital Properties with Respect to the LMC in MW1 Using the LMC3 Model

Name	$f_{\text{peri},1}$	$f_{\text{router},1}$	$r_{\text{peri},1}$ (kpc)	$t_{\text{peri},1}$ (Gyr)	$f_{\text{apo},1}$	$r_{\text{apo},1}$ (kpc)	$t_{\text{apo},1}$ (Gyr)
Most recent							
Aqu2	1.0	0.71	60.96 ± 20.06	0.16 ± 0.06	0.22	452.5 ± 158.17	2.98 ± 1.16
CanVen2	0.27	0.02	226.94 ± 120.08	3.39 ± 1.24	0.33	338.6 ± 108.02	1.77 ± 1.24
Car2	0.87	0.82	30.96 ± 42.7	1.13 ± 0.47	0.9	74.11 ± 80.0	0.61 ± 0.84
Car3	1.0	1.0	8.75 ± 2.98	0.18 ± 0.05	1.0	52.89 ± 32.46	0.87 ± 0.36
Cra2	1.0	0.06	231.45 ± 92.57	2.78 ± 0.89	1.0	338.84 ± 46.2	1.43 ± 0.21
Dra2	0.33	0.03	292.17 ± 186.9	4.53 ± 1.13	0.63	529.19 ± 155.54	3.16 ± 1.12
Hor1	0.98	0.98	30.92 ± 13.45	0.31 ± 0.38	0.94	114.81 ± 150.67	1.38 ± 1.27
Hyi1	1.0	1.0	11.49 ± 2.35	0.26 ± 0.03	1.0	29.37 ± 2.4	0.72 ± 0.06
Hya2	0.27	0.03	130.97 ± 40.22	0.99 ± 1.28	0.17	241.56 ± 152.22	1.24 ± 1.56
Phx2	0.98	0.97	32.99 ± 17.76	0.49 ± 0.49	0.94	157.54 ± 164.04	2.04 ± 1.26
Ret2	1.0	1.0	15.57 ± 2.93	0.13 ± 0.02	0.95	154.62 ± 189.67	1.62 ± 1.37
Seg1	1.0	0.93	55.74 ± 10.63	0.32 ± 0.11	1.0	70.02 ± 7.18	0.11 ± 0.04
Tuc3	1.0	1.0	14.76 ± 3.25	0.08 ± 0.01	0.72	210.6 ± 140.48	1.22 ± 1.01
Car1	0.74	0.13	115.56 ± 115.01	1.58 ± 1.13	0.95	235.88 ± 207.05	1.62 ± 1.7
Dra1	0.67	0.08	279.59 ± 140.87	4.51 ± 0.97	0.97	424.29 ± 92.17	2.64 ± 0.54
Fnx1	1.0	0.0	99.93 ± 4.73	0.15 ± 0.08	0.88	318.34 ± 240.72	2.53 ± 2.04
Scu1	1.0	1.0	28.81 ± 4.87	0.11 ± 0.01	0.89	330.82 ± 91.61	2.06 ± 0.84
UMin1	0.79	0.13	258.84 ± 132.6	4.13 ± 1.06	0.98	392.29 ± 67.75	2.31 ± 0.42
Name	$f_{\text{peri},2}$	$f_{\text{router},2}$	$r_{\text{peri},2}$ (kpc)	$t_{\text{peri},2}$ (Gyr)	$f_{\text{apo},2}$	$r_{\text{apo},2}$ (kpc)	$t_{\text{apo},2}$ (Gyr)
Second to last							
Aqu2	1.0	0.01	305.78 ± 163.31	4.13 ± 1.04	0.08	358.57 ± 125.89	4.74 ± 0.82
CanVen2	0.27	0.0	231.59 ± 95.9	4.75 ± 0.87	0.1	326.49 ± 111.18	4.78 ± 1.0
Car2	0.87	0.64	36.12 ± 42.96	3.75 ± 0.97	0.82	119.57 ± 91.3	2.76 ± 0.97
Car3	1.0	0.98	7.51 ± 10.96	1.54 ± 0.69	0.95	52.58 ± 21.17	2.15 ± 0.73
Cra2	1.0	0.01	366.44 ± 191.27	4.87 ± 0.7	0.84	389.8 ± 156.15	4.59 ± 0.73
Dra2	0.33	0.0	356.7 ± 176.3	5.11 ± 0.71	0.07	391.59 ± 143.6	4.93 ± 0.75
Hor1	0.98	0.76	46.11 ± 92.67	1.92 ± 1.21	0.78	73.33 ± 81.39	2.51 ± 1.19
Hyi1	1.0	1.0	7.83 ± 2.1	1.15 ± 0.11	1.0	27.76 ± 5.06	1.55 ± 0.17
Hya2	0.27	0.0	159.45 ± 47.16	4.63 ± 1.11	0.07	365.61 ± 151.89	4.06 ± 1.1
Phx2	0.98	0.64	67.03 ± 121.01	2.74 ± 1.2	0.66	96.48 ± 107.71	3.44 ± 1.06
Ret2	1.0	0.68	91.36 ± 171.87	2.09 ± 1.33	0.81	120.01 ± 166.05	2.59 ± 1.24
Seg1	1.0	0.01	212.87 ± 120.51	1.77 ± 1.01	0.98	240.9 ± 129.01	1.39 ± 0.91
Tuc3	1.0	0.04	174.36 ± 102.45	1.4 ± 1.18	0.54	267.85 ± 135.58	2.09 ± 1.42
Car1	0.74	0.14	127.28 ± 91.4	4.31 ± 1.03	0.61	229.62 ± 114.04	3.64 ± 1.13
Dra1	0.67	0.0	326.4 ± 14.86	4.23 ± 0.51	0.04	432.25 ± 211.38	5.38 ± 0.64
Fnx1	1.0	0.09	98.94 ± 44.37	1.54 ± 0.78	0.46	232.8 ± 78.98	3.78 ± 0.82
Scu1	1.0	0.28	136.77 ± 115.49	4.25 ± 0.92	0.26	257.26 ± 52.52	5.15 ± 0.65
UMin1	0.79	0.0	277.26 ± 52.98	4.8 ± 0.93	0.18	495.87 ± 190.92	5.5 ± 0.54

Table B2
Orbital Properties with Respect to the LMC in MW2 Using the LMC3 Model

Name	$f_{\text{peri},1}$	$f_{\text{router},1}$	$r_{\text{peri},1}$ (kpc)	$t_{\text{peri},1}$ (Gyr)	$f_{\text{apo},1}$	$r_{\text{apo},1}$ (kpc)	$t_{\text{apo},1}$ (Gyr)
Most recent							
Aqu2	1.0	0.9	60.86 \pm 19.92	0.16 \pm 0.06	0.36	369.57 \pm 159.98	1.98 \pm 0.8
CanVen2	0.5	0.07	181.89 \pm 96.91	2.24 \pm 1.03	0.54	292.48 \pm 97.44	1.04 \pm 1.14
Car2	1.0	0.84	72.08 \pm 107.47	1.3 \pm 1.2	1.0	103.24 \pm 121.29	0.76 \pm 0.98
Car3	1.0	1.0	8.1 \pm 3.0	0.18 \pm 0.05	1.0	47.55 \pm 27.41	0.77 \pm 0.26
Cra2	1.0	0.24	134.93 \pm 62.04	2.28 \pm 0.58	1.0	265.35 \pm 30.15	0.94 \pm 0.14
Dra2	0.95	0.14	159.49 \pm 85.59	3.24 \pm 1.01	0.99	326.01 \pm 106.52	1.54 \pm 0.56
Hor1	0.98	0.98	34.25 \pm 17.33	0.26 \pm 0.44	0.98	106.46 \pm 119.89	1.2 \pm 1.19
Hyi1	1.0	1.0	10.79 \pm 2.4	0.26 \pm 0.03	1.0	33.17 \pm 4.76	0.75 \pm 0.1
Hya2	0.33	0.05	156.7 \pm 128.68	1.25 \pm 1.59	0.24	293.93 \pm 200.07	1.52 \pm 1.66
Phx2	0.97	0.96	37.34 \pm 22.2	0.42 \pm 0.53	0.98	146.69 \pm 133.48	1.78 \pm 1.25
Ret2	1.0	1.0	15.32 \pm 3.03	0.13 \pm 0.02	1.0	181.5 \pm 128.26	1.62 \pm 0.93
Seg1	1.0	1.0	48.96 \pm 8.77	0.29 \pm 0.08	1.0	68.29 \pm 6.27	0.09 \pm 0.03
Tuc3	1.0	1.0	15.08 \pm 3.24	0.07 \pm 0.01	0.84	164.48 \pm 117.1	0.95 \pm 0.85
Car1	0.97	0.38	77.53 \pm 56.63	1.35 \pm 0.85	1.0	134.41 \pm 84.32	0.68 \pm 0.67
Dra1	0.78	0.21	156.11 \pm 95.25	3.87 \pm 1.14	0.9	290.96 \pm 53.55	1.98 \pm 0.89
Fnx1	1.0	0.0	100.64 \pm 3.91	0.13 \pm 0.03	1.0	188.88 \pm 142.66	1.22 \pm 1.18
Scu1	1.0	1.0	29.1 \pm 4.95	0.11 \pm 0.01	1.0	221.94 \pm 47.15	1.04 \pm 0.25
UMin1	0.89	0.24	148.29 \pm 84.61	3.64 \pm 1.06	0.96	273.14 \pm 43.12	1.74 \pm 0.77
Name	$f_{\text{peri},1}$	$f_{\text{router},2}$	$r_{\text{peri},2}$ (kpc)	$t_{\text{peri},2}$ (Gyr)	$f_{\text{apo},2}$	$r_{\text{apo},2}$ (kpc)	$t_{\text{apo},2}$ (Gyr)
Second to last							
Aqu2	0.34	0.05	239.75 \pm 175.98	3.41 \pm 0.99	0.2	293.09 \pm 121.33	4.21 \pm 0.93
CanVen2	0.22	0.08	127.12 \pm 134.84	4.72 \pm 0.78	0.37	380.28 \pm 185.18	4.0 \pm 0.84
Car2	0.86	0.08	151.68 \pm 52.0	3.88 \pm 0.89	0.97	258.48 \pm 94.63	3.07 \pm 0.98
Car3	1.0	1.0	6.74 \pm 8.18	1.36 \pm 0.52	0.98	55.35 \pm 37.18	2.07 \pm 0.75
Cra2	0.8	0.1	155.33 \pm 82.4	4.38 \pm 0.94	0.93	239.43 \pm 105.62	3.56 \pm 0.78
Dra2	0.35	0.01	174.94 \pm 79.61	4.72 \pm 0.81	0.59	293.11 \pm 105.52	4.33 \pm 0.96
Hor1	0.89	0.74	46.15 \pm 64.79	1.69 \pm 1.27	0.8	90.62 \pm 92.33	2.31 \pm 1.2
Hyi1	1.0	1.0	3.76 \pm 2.26	1.2 \pm 0.18	1.0	35.79 \pm 10.9	1.67 \pm 0.28
Hya2	0.11	0.02	153.15 \pm 95.69	4.38 \pm 0.96	0.14	327.82 \pm 145.06	3.3 \pm 1.02
Phx2	0.85	0.62	67.32 \pm 81.05	2.37 \pm 1.17	0.72	130.55 \pm 108.4	3.27 \pm 1.13
Ret2	0.98	0.48	109.54 \pm 106.68	2.41 \pm 1.27	0.85	185.42 \pm 140.22	3.0 \pm 1.23
Seg1	1.0	0.09	136.35 \pm 52.78	1.29 \pm 0.5	1.0	170.25 \pm 54.15	0.92 \pm 0.35
Tuc3	0.82	0.2	122.9 \pm 67.91	1.19 \pm 0.88	0.72	219.52 \pm 118.4	1.96 \pm 1.24
Car1	0.72	0.24	123.55 \pm 77.41	3.43 \pm 1.1	0.84	183.86 \pm 93.43	2.79 \pm 1.13
Dra1	0.12	0.0	192.53 \pm 75.39	5.09 \pm 0.9	0.35	316.99 \pm 143.2	4.66 \pm 0.77
Fnx1	0.93	0.3	105.01 \pm 53.94	1.85 \pm 1.42	0.78	202.39 \pm 80.26	2.77 \pm 0.68
Scu1	1.0	0.72	75.04 \pm 66.9	2.45 \pm 0.54	0.99	261.89 \pm 96.32	3.81 \pm 0.75
UMin1	0.21	0.01	210.5 \pm 95.03	5.22 \pm 0.63	0.48	297.87 \pm 145.48	4.53 \pm 0.66

Appendix C

Orbital Properties with Respect to the Milky Way


Table C1 shows the statistical significance of orbital properties for all candidate Magellanic satellites in LMC2 with respect to MW1 (top) and MW2 (bottom).

Table C1
Orbital Properties with Respect to the MW for the Fiducial LMC Model

Name	$f_{\text{peri},1}$	$r_{\text{peri},1}$ (kpc)	$t_{\text{peri},1}$ (Gyr)	$f_{\text{apo},1}$	$r_{\text{apo},1}$ (kpc)	$t_{\text{apo},1}$ (Gyr)
MW1						
Aqu2	0.91	93.31 ± 24.3	0.17 ± 0.23	0.19	208.13 ± 87.52	2.86 ± 1.13
CanVen2	0.13	59.29 ± 83.27	4.64 ± 0.79	0.25	349.77 ± 96.71	3.01 ± 1.32
Car2	1.0	28.05 ± 1.25	0.08 ± 0.01	0.93	318.46 ± 120.33	3.24 ± 1.19
Car3	1.0	28.81 ± 1.26	0.01 ± 0.0	0.88	395.63 ± 121.82	3.46 ± 1.01
Cra2	1.0	18.95 ± 9.65	2.06 ± 0.34	1.0	143.23 ± 11.6	0.76 ± 0.17
Dra2	0.39	31.86 ± 21.61	3.75 ± 1.2	0.55	246.86 ± 97.34	2.53 ± 1.25
Hor1	0.87	181.39 ± 138.95	1.58 ± 1.43	0.92	205.97 ± 144.31	1.28 ± 1.39
Hyl1	0.95	344.25 ± 106.06	3.06 ± 0.47	0.95	361.46 ± 100.55	2.67 ± 0.52
Hya2	1.0	133.21 ± 24.97	0.18 ± 0.21	0.08	275.88 ± 69.99	3.79 ± 0.94
Phx2	0.7	198.82 ± 143.23	2.55 ± 1.67	0.87	263.21 ± 141.79	2.15 ± 1.47
Ret2	0.81	165.96 ± 160.3	3.35 ± 1.26	0.96	259.06 ± 147.94	2.47 ± 1.18
Seg1	1.0	19.62 ± 5.12	0.1 ± 0.02	1.0	63.89 ± 34.84	0.67 ± 0.32
Tuc3	0.99	2.01 ± 1.8	0.64 ± 0.12	0.99	52.11 ± 13.76	0.3 ± 0.15
Car1	1.0	80.14 ± 18.25	0.78 ± 0.19	0.99	146.66 ± 54.19	1.52 ± 1.53
Dra1	1.0	84.94 ± 19.16	2.8 ± 0.78	1.0	137.06 ± 26.52	1.21 ± 0.42
Fnx1	0.91	108.09 ± 25.51	1.37 ± 0.26	0.99	160.39 ± 51.56	0.59 ± 1.19
Scu1	1.0	57.21 ± 6.24	0.37 ± 0.04	0.96	296.98 ± 55.37	3.49 ± 0.71
UMin1	1.0	77.05 ± 16.17	2.52 ± 0.66	1.0	124.18 ± 22.28	1.08 ± 0.39
Name	$f_{\text{peri},1}$	$r_{\text{peri},1}$ (kpc)	$t_{\text{peri},1}$ (Gyr)	$f_{\text{apo},1}$	$r_{\text{apo},1}$ (kpc)	$t_{\text{apo},1}$ (Gyr)
MW2						
Aqu2	0.91	91.9 ± 25.56	0.18 ± 0.22	0.29	230.05 ± 107.51	2.62 ± 1.04
CanVen2	0.3	81.13 ± 79.04	3.88 ± 1.0	0.4	306.97 ± 82.59	2.1 ± 1.03
Car2	1.0	27.55 ± 1.3	0.08 ± 0.01	1.0	145.95 ± 30.25	1.28 ± 0.36
Car3	1.0	29.09 ± 9.2	0.02 ± 0.15	1.0	251.66 ± 83.71	2.19 ± 0.73
Cra2	1.0	17.93 ± 8.75	1.55 ± 0.19	1.0	132.0 ± 8.09	0.51 ± 0.09
Dra2	0.92	31.81 ± 13.0	2.61 ± 1.15	0.98	177.78 ± 91.76	1.45 ± 0.87
Hor1	0.93	112.34 ± 75.01	1.36 ± 1.32	0.98	153.1 ± 96.13	0.9 ± 1.13
Hyl1	0.94	184.14 ± 86.37	3.12 ± 1.26	1.0	251.17 ± 94.39	2.19 ± 0.75
Hya2	1.0	131.85 ± 26.96	0.19 ± 0.21	0.15	252.34 ± 71.86	3.22 ± 0.93
Phx2	0.92	106.58 ± 63.79	2.13 ± 1.65	0.97	176.07 ± 95.04	1.29 ± 1.12
Ret2	1.0	59.68 ± 44.63	2.09 ± 0.98	1.0	116.76 ± 68.53	1.19 ± 0.64
Seg1	1.0	18.82 ± 5.23	0.1 ± 0.02	1.0	50.71 ± 18.8	0.51 ± 0.14
Tuc3	0.99	2.09 ± 1.81	0.49 ± 0.12	1.0	45.57 ± 21.66	0.23 ± 0.21
Car1	1.0	67.04 ± 17.79	0.82 ± 0.1	1.0	133.58 ± 29.83	1.35 ± 1.1
Dra1	1.0	67.93 ± 14.3	1.67 ± 0.34	1.0	108.96 ± 13.31	0.64 ± 0.18
Fnx1	0.99	87.33 ± 24.96	1.32 ± 0.31	1.0	146.22 ± 10.88	0.22 ± 0.33
Scu1	1.0	53.12 ± 6.27	0.37 ± 0.03	1.0	198.38 ± 23.77	2.06 ± 0.24
UMin1	1.0	63.45 ± 13.0	1.54 ± 0.29	1.0	100.67 ± 9.79	0.57 ± 0.17

Note. Orbital parameters calculated with respect to the MW. All values are still calculated for the fiducial LMC model. Columns 1–8 provide the results in the MW1 potential, and Columns 9–16 list results for MW2.

ORCID iDs

Ekta Patel  <https://orcid.org/0000-0002-9820-1219>
 Nitya Kallivayalil  <https://orcid.org/0000-0002-3204-1742>
 Nicolas Garavito-Camargo  <https://orcid.org/0000-0001-7107-1744>
 Daniel R. Weisz  <https://orcid.org/0000-0002-6442-6030>
 Roeland P. van der Marel  <https://orcid.org/0000-0001-7827-7825>
 Michael Boylan-Kolchin  <https://orcid.org/0000-0002-9604-343X>
 Marcel S. Pawlowski  <https://orcid.org/0000-0002-9197-9300>
 Facundo A. Gómez  <https://orcid.org/0000-0002-1947-333X>

References

- Battaglia, G., Irwin, M., Tolstoy, E., de Boer, T., & Mateo, M. 2012, *ApJL*, **761**, L31
- Battaglia, G., Tolstoy, E., Helmi, A., et al. 2006, *A&A*, **459**, 423
- Bechtol, K., Drlica-Wagner, A., Balbinot, E., et al. 2015, *ApJ*, **807**, 50
- Bekki, K., & Chiba, M. 2005, *MNRAS*, **356**, 680
- Bellazzini, M., Ferraro, F. R., Origlia, L., et al. 2002, *AJ*, **124**, 3222
- Belokurov, V., Zucker, D. B., Evans, N. W., et al. 2007, *ApJ*, **654**, 897
- Besla, G. 2015, arXiv:1511.03346
- Besla, G., Hernquist, L., & Loeb, A. 2013, *MNRAS*, **428**, 2342
- Besla, G., Kallivayalil, N., Hernquist, L., et al. 2007, *ApJ*, **668**, 949
- Besla, G., Kallivayalil, N., Hernquist, L., et al. 2010, *ApJL*, **721**, L97
- Besla, G., Kallivayalil, N., Hernquist, L., et al. 2012, *MNRAS*, **421**, 2109
- Besla, G., Martínez-Delgado, D., van der Marel, R. P., et al. 2016, *ApJ*, **825**, 20
- Bonanos, A. Z., Stanek, K. Z., Szentgyorgyi, A. H., Sasselov, D. D., & Bakos, G. Á. 2004, *AJ*, **127**, 861
- Boylan-Kolchin, M., Besla, G., & Hernquist, L. 2011, *MNRAS*, **414**, 1560
- Brown, T. M., Tumlinson, J., Geha, M., et al. 2014, *MmSAI*, **85**, 493
- Bryan, G. L., & Norman, M. L. 1998, *ApJ*, **495**, 80
- Bullock, J. S., & Boylan-Kolchin, M. 2017, *ARA&A*, **55**, 343
- Caldwell, N., Walker, M. G., Mateo, M., et al. 2017, *ApJ*, **839**, 20
- Carrera, R., Aparicio, A., Martínez-Delgado, D., & Alonso-García, J. 2002, *AJ*, **123**, 3199
- Chandrasekhar, S. 1943, *ApJ*, **97**, 255
- Cioni, M. R. L., van der Marel, R. P., Loup, C., & Habing, H. J. 2000, *A&A*, **359**, 601
- Coppola, G., Marconi, M., Stetson, P. B., et al. 2015, *ApJ*, **814**, 71
- Deason, A. J., Wetzel, A. R., Garrison-Kimmel, S., & Belokurov, V. 2015, *MNRAS*, **453**, 3568
- Di Teodoro, E. M., McClure-Griffiths, N. M., Jameson, K. E., et al. 2019, *MNRAS*, **483**, 392
- D'Onghia, E., & Lake, G. 2008, *ApJL*, **686**, L61
- Dooley, G. A., Peter, A. H. G., Carlin, J. L., et al. 2017, *MNRAS*, **472**, 1060
- Drlica-Wagner, A., Bechtol, K., Allam, S., et al. 2016, *ApJL*, **833**, L5
- Drlica-Wagner, A., Bechtol, K., Rykoff, E. S., et al. 2015, *ApJ*, **813**, 109
- Erkal, D., & Belokurov, V. A. 2019, arXiv:1907.09484
- Erkal, D., Li, T. S., Koposov, S. E., et al. 2018, *MNRAS*, **481**, 3148
- Fattahi, A., Navarro, J. F., Frenk, C. S., et al. 2018, *MNRAS*, **476**, 3816
- Freedman, W. L., Madore, B. F., Gibson, B. K., et al. 2001, *ApJ*, **553**, 47
- Fritz, T. K., Battaglia, G., Pawlowski, M. S., et al. 2018, *A&A*, **619**, A103
- Fritz, T. K., Carrera, R., Battaglia, G., & Taibi, S. 2019, *A&A*, **623**, A129
- Fu, S. W., Simon, J. D., & Alarcón Jara, A. G. 2019, *ApJ*, **883**, 11
- Gaia Collaboration, Brown, A. G. A., Vallenari, A., et al. 2018a, *A&A*, **616**, A1
- Gaia Collaboration, Helmi, A., van Leeuwen, F., et al. 2018b, *A&A*, **616**, A12
- Garavito-Camargo, N., Besla, G., Laporte, C. F. P., et al. 2019, *ApJ*, **884**, 51
- Gnedin, O. Y., Kravtsov, A. V., Klypin, A. A., & Nagai, D. 2004, *ApJ*, **616**, 16
- Gómez, F. A., Besla, G., Carpintero, D. D., et al. 2015, *ApJ*, **802**, 128
- Groco, C., Dall'Ora, M., Clementini, G., et al. 2008, *ApJL*, **675**, L73
- Harris, J., & Zaritsky, D. 2006, *AJ*, **131**, 2514
- Hashimoto, Y., Funato, Y., & Makino, J. 2003, *ApJ*, **582**, 196
- Hernquist, L. 1990, *ApJ*, **356**, 359
- Homma, D., Chiba, M., Okamoto, S., et al. 2018, *PASJ*, **70**, S18
- Hunter, J. D. 2007, *CSE*, **9**, 90
- Jahn, E. D., Sales, L. V., Wetzel, A., et al. 2019, *MNRAS*, **489**, 5348
- Jeon, M., Besla, G., & Bromm, V. 2017, *ApJ*, **848**, 85
- Jethwa, P., Erkal, D., & Belokurov, V. 2016, *MNRAS*, **461**, 2212
- Ji, A. P., Frebel, A., Simon, J. D., & Chiti, A. 2016, *ApJ*, **830**, 93
- Ji, A. P., Li, T. S., Simon, J. D., et al. 2019, *ApJ*, **889**, 27
- Jones, E., Oliphant, T., Peterson, P., et al. 2001, SciPy: Open Source Scientific Tools for Python (USA: Trelgol Publishing), <http://www.scipy.org/>
- Joo, S.-J., Kyeong, J., Yang, S.-C., et al. 2018, *ApJ*, **861**, 23
- Kallivayalil, N., Sales, L. V., Zivick, P., et al. 2018, *ApJ*, **867**, 19
- Kallivayalil, N., van der Marel, R. P., Besla, G., Anderson, J., & Alcock, C. 2013, *ApJ*, **764**, 161
- Kim, D., & Jerjen, H. 2015, *ApJL*, **808**, L39
- Kim, D., Jerjen, H., Mackey, D., Da Costa, G. S., & Milone, A. P. 2015, *ApJL*, **804**, L44
- Kinemuchi, K., Harris, H. C., Smith, H. A., et al. 2008, *AJ*, **136**, 1921
- Kirby, E. N., Guhathakurta, P., Simon, J. D., et al. 2010, *ApJS*, **191**, 352
- Kirby, E. N., Simon, J. D., & Cohen, J. G. 2015, *ApJ*, **810**, 56
- Koposov, S. E., Belokurov, V., Torrealba, G., & Evans, N. W. 2015a, *ApJ*, **805**, 130
- Koposov, S. E., Casey, A. R., Belokurov, V., et al. 2015b, *ApJ*, **811**, 62
- Koposov, S. E., Walker, M. G., Belokurov, V., et al. 2018, *MNRAS*, **479**, 5343
- Laevens, B. P. M., Martin, N. F., Ibata, R. A., et al. 2015, *ApJL*, **802**, L18
- Li, T. S., Simon, J. D., Kuehn, K., et al. 2018a, *ApJ*, **866**, 22
- Li, T. S., Simon, J. D., Pace, A. B., et al. 2018b, *ApJ*, **857**, 145
- Longard, N., Martin, N., Starkenburg, E., et al. 2018, *MNRAS*, **480**, 2609
- Lynden-Bell, D. 1976, *MNRAS*, **174**, 695
- Martin, N. F., Ibata, R. A., Lewis, G. F., et al. 2016, *ApJ*, **833**, 167
- Martin, N. F., Nidever, D. L., Besla, G., et al. 2015, *ApJL*, **804**, L5
- Martínez-Vázquez, C. E., Stetson, P. B., Monelli, M., et al. 2016, *MNRAS*, **462**, 4349
- Massari, D., & Helmi, A. 2018, *A&A*, **620**, A155
- McMillan, P. J. 2011, *MNRAS*, **418**, 1565
- Miyamoto, M., & Nagai, R. 1975, *PASJ*, **27**, 533
- Muñoz, R. R., Côté, P., Santana, F. A., et al. 2018, *ApJ*, **860**, 66
- Murai, T., & Fujimoto, M. 1980, *PASJ*, **32**, 581
- Mutlu-Pakdil, B., Sand, D. J., Carlin, J. L., et al. 2018, *ApJ*, **863**, 25
- Nadler, E. O., Wechsler, R. H., Bechtol, K., et al. 2019, arXiv:1912.03303
- Nagasawa, D. Q., Marshall, J. L., Li, T. S., et al. 2018, *ApJ*, **852**, 99
- Navarro, J. F., Frenk, C. S., & White, S. D. M. 1996, *ApJ*, **462**, 563
- Pace, A. B., & Li, T. S. 2019, *ApJ*, **875**, 77
- Pardy, S. A., D'Onghia, E., Navarro, J., et al. 2020, *MNRAS*, **492**, 1543
- Patel, E., Besla, G., & Sohn, S. T. 2017, *MNRAS*, **464**, 3825
- Patel, E., Carlin, J. L., Tollerud, E. J., Collins, M. L. M., & Dooley, G. A. 2018, *MNRAS*, **480**, 1883
- Pawlowski, M. S., & Kroupa, P. 2019, *MNRAS*, **491**, 3042
- Pawlowski, M. S., Pflamm-Altenburg, J., & Kroupa, P. 2012, *MNRAS*, **423**, 1109
- Piatek, S., Pryor, C., Bristow, P., et al. 2005, *AJ*, **130**, 95
- Piatek, S., Pryor, C., Bristow, P., et al. 2007, *AJ*, **133**, 818
- Piatek, S., Pryor, C., Olszewski, E. W., et al. 2003, *AJ*, **126**, 2346
- Pietrzyński, G., Gieren, W., Szczygłowski, O., et al. 2008, *AJ*, **135**, 1993
- Plummer, H. C. 1911, *MNRAS*, **71**, 460
- Rizzi, L., Held, E. V., Saviane, I., Tully, R. B., & Gullieuszik, M. 2007, *MNRAS*, **380**, 1255
- Sales, L. V., Navarro, J. F., Cooper, A. P., et al. 2011, *MNRAS*, **418**, 648
- Sales, L. V., Navarro, J. F., Kallivayalil, N., & Frenk, C. S. 2017, *MNRAS*, **465**, 1879
- Sales, L. V., Wang, W., White, S. D. M., & Navarro, J. F. 2013, *MNRAS*, **428**, 573
- Sanders, J. L., Evans, N. W., & Dehnen, W. 2018, *MNRAS*, **478**, 3879
- Santistevan, I. B., Wetzel, A., El-Badry, K., et al. 2020, arXiv:2001.03178
- Schönrich, R., Binney, J., & Dehnen, W. 2010, *MNRAS*, **403**, 1829
- Simon, J. D. 2018, *ApJ*, **863**, 89
- Simon, J. D., Drlica-Wagner, A., Li, T. S., et al. 2015, *ApJ*, **808**, 95
- Simon, J. D., & Geha, M. 2007, *ApJ*, **670**, 313
- Simon, J. D., Geha, M., Minor, Q. E., et al. 2011, *ApJ*, **733**, 46
- Simon, J. D., Li, T. S., Drlica-Wagner, A., et al. 2017, *ApJ*, **838**, 11
- Sohn, S. T., Patel, E., Besla, G., et al. 2017, *ApJ*, **849**, 93
- Springel, V., Yoshida, N., & White, S. D. M. 2001, *NewA*, **6**, 79
- The Astropy Collaboration, Price-Whelan, A. M., Sipőcz, B. M., et al. 2018, arXiv:1801.02634
- Torrealba, G., Belokurov, V., Koposov, S. E., et al. 2018, *MNRAS*, **475**, 5085
- Torrealba, G., Koposov, S. E., Belokurov, V., & Irwin, M. 2016a, *MNRAS*, **459**, 2370
- Torrealba, G., Koposov, S. E., Belokurov, V., et al. 2016b, *MNRAS*, **463**, 712
- van der Marel, R. P., Alves, D. R., Hardy, E., & Suntzeff, N. B. 2002, *AJ*, **124**, 2639
- van der Marel, R. P., Besla, G., Cox, T. J., Sohn, S. T., & Anderson, J. 2012a, *ApJ*, **753**, 9

- van der Marel, R. P., Fardal, M., Besla, G., et al. 2012b, [ApJ](#), **753**, 8
- van der Marel, R. P., & Kallivayalil, N. 2014, [ApJ](#), **781**, 121
- van der Walt, S., Colbert, S. C., & Varoquaux, G. 2011, [CSE](#), **13**, 22
- Vivas, A. K., & Mateo, M. 2013, [AJ](#), **146**, 141
- Vivas, A. K., Olsen, K., Blum, R., et al. 2016, [AJ](#), **151**, 118
- Walker, M. G., Mateo, M., & Olszewski, E. W. 2008, [ApJL](#), **688**, L75
- Walker, M. G., Mateo, M., & Olszewski, E. W. 2009a, [AJ](#), **137**, 3100
- Walker, M. G., Mateo, M., Olszewski, E. W., et al. 2009b, [ApJ](#), **704**, 1274
- Walker, M. G., Mateo, M., Olszewski, E. W., et al. 2015, [ApJ](#), **808**, 108
- Weisz, D. R., Dolphin, A. E., Skillman, E. D., et al. 2014, [ApJ](#), **789**, 147
- Zentner, A. R., & Bullock, J. S. 2003, [ApJ](#), **598**, 49
- Zhao, H. 1998, [ApJL](#), **500**, L149
- Zivick, P., Kallivayalil, N., van der Marel, R. P., et al. 2018, [ApJ](#), **864**, 55